EUROPEAN ORGANIZATION FOR NUCLEAR RESEARCH


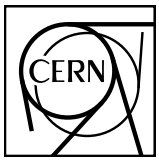


ALICE-PUBLIC-2020-005
CERN-LHCC-2020-018; LHCC-G-179

# Future high-energy pp programme with ALICE

ALICE Collaboration *

**Abstract**

This document presents the proposal of the ALICE Collaboration for an extended data taking programme with high-energy proton–proton collisions ($\sqrt{s} \approx$ 13–14 TeV). The proposed programme includes two components: a sample with a target integrated luminosity of about 200 pb$^{-1}$, for which a highly-selective software-based event skimming will be performed after data reconstruction, and a minimum bias sample with a target integrated luminosity of about 3 pb$^{-1}$. The first sample targets several physics topics based on the selection of rare events, in particular with very high particle multiplicity or diffractive topologies, and/or rare signals, ranging from light nuclei and hyperons to heavy-quark hadrons and jets. The data processing and selection strategy exploits the new online–offline computing framework that is being prepared to process the Pb–Pb data samples. The second sample will be recorded with a reduced value of the ALICE solenoid magnetic field (0.2 T) and will be devoted to high-precision studies of low-mass dielectron pairs.



*See Appendix A for the full list of Collaborations members.

## Contents

## 1 Executive summary

The ALICE detector is presently undergoing a major upgrade in view of data taking during the LHC Runs 3 and 4 [1]. The main elements of the apparatus upgrade include: the replacement of the Inner Tracking System (ITS) with a completely new detector based on Monolithic Active Pixel Sensors (MAPS), the replacement of the Time Projection Chamber (TPC) readout with GEM detectors, the addition of a MAPS-based Muon Forward Tracker (MFT) in front the Muon Spectrometer, and the implementation of new Fast Interaction Trigger (FIT) detector. In addition, the readout of several other detectors (Time Of Flight, Muon Identifier, Muon Tracker) is being upgraded and a new Online–Offline system ($O^2$) for data recording, compression, calibration and reconstruction is being implemented. The new apparatus with the $O^2$ system will record Pb–Pb collisions at an interaction rate of up to 50 kHz with most of the detectors operating in continuous readout mode, i.e. providing a continuous stream of data to the $O^2$ system, in which reconstructed tracks and detector signals will be associated to the individual collision events. For proton–proton collisions, the experiment can in principle be operated at an interaction rate of up to 4 MHz, which gives the same particle rate as Pb–Pb collisions at 50 kHz. An interaction rate of 0.5–1 MHz is considered as a suitable working point in order to limit the pile-up of collisions within the ITS readout time to a number (2–5 collisions) that can be separated without ambiguity using the track association to reconstructed primary vertices. For this document, an interaction rate of 0.5 MHz is assumed as a baseline, corresponding to an instantaneous luminosity of about $6 \times 10^{30}$ s$^{-1}$cm$^{-2}$. While such instantaneous luminosity is larger by about a factor five with respect to the typical values used for ALICE in Run 2, similar values were already reached during Run 2 hence there are no special requirements on the beam setup. This increase, combined with the large increase of the readout speed, allows for the inspection of a data sample with an integrated luminosity larger by a factor 5–20 for those measurements that used rare triggers in Run 2, and by almost three orders of magnitude for those measurements that, not having a suitable hardware trigger, were performed using a pre-scaled minimum bias trigger in Run 2. In addition, the tracking performance of the new apparatus, with vertexing resolution improved by a factor three for central barrel tracks and newly-added vertexing capabilities for forward muons, will strongly enhance measurements in the sectors of heavy flavour, quarkonia, low-mass dielectrons and hyper-nuclei [2].

The ALICE data taking programme that was proposed in 2012 [1] together with the detector upgrade was focused on heavy-ion campaigns (Pb–Pb and p–Pb) and corresponding pp reference data samples at the same centre-of-mass energy, and it included data taking with high-energy pp collisions for only a few months per year. The present proposal extends the high-energy pp programme to essentially the full LHC operation period during Run 3 and, possibly, part of Run 4.

The main physics motivations for an extended pp programme are presented in this document (Section 2) and can be grouped in the following four main headers. The first item (high-density QCD studies) builds on the discussions that took place during the HL-LHC Physics Workshop 2017–18, which are summarised in the Working Group 5 (High-density QCD) report [3].

– **High-density QCD effects and search for quark–gluon plasma in high-multiplicity pp collisions.** The discovery of heavy-ion-like phenomena —in particular, the long-range correlation structures (the *ridge*) and the increasing production of strangeness as a function of multiplicity— in the small collision systems, pp and p–Pb, has been a major outcome of the LHC programme so far, and one of the most unexpected. A data sample with selection of high-multiplicity events and an integrated luminosity of about 200 pb$^{-1}$ would be larger by a factor of 10 with respect to the sample recorded during Run 2. Such increase would allow us to a) study pp collisions with a multiplicity of charged particles per unit of pseudorapidity $\mathrm{d}N_{\mathrm{ch}}/\mathrm{d}\eta \approx 100$ as found in semi-peripheral Pb–Pb collisions and an estimated energy density $\varepsilon \sim 50$ GeV/fm$^3$ as found in central Pb–Pb collisions; b) search for jet quenching, one of the characterising quark–gluon plasma (QGP) signatures that has not been observed so far in small-system collisions, with a sensitivity to energy

losses of 20–100 MeV, depending on the multiplicity selection.

– **Light nuclei and hyper-nuclei production, hadron–hadron interactions, and their astrophysical implications.** Studying light nuclei and hyper-nuclei will give insight into production cross sections and production mechanisms with a direct impact on Dark Matter searches in Space. Indeed, the poor knowledge of the production yields of nuclei in ordinary cosmic-ray-induced hadronic collisions in Space is one of the main limitations for the search for Dark Matter annihilating to nucleus–antinucleus pairs. An integrated luminosity of 200 pb$^{-1}$ would enable one to observe for the first time and characterise the momentum-differential production of $^{4}\overline{\mathrm{He}}$ with a precision of about 10%, as well as to close the case on the yet-unknown production mechanism of hyper-nuclei such as $^{3}_{\Lambda}$H. These nuclei would be selected after full event reconstruction, exploiting the entire delivered luminosity. The study of two-particle correlations in momentum space has proven to provide direct access to the interaction between nucleons and hyperons (strange baryons), between hyperon pairs, and between kaons and light nuclei; besides its intrinsic interest, this study has clear implications for the nature and equation of state of matter in dense neutron stars. An integrated luminosity of 200 pb$^{-1}$ would also provide precise information on the p–$\Sigma^0$ potential and open first studies of the $\Omega$–$\Omega$ potential.

– **New and reference measurements of rare QCD processes (heavy quarks, jets, central diffraction).** Exploiting the event selection after full reconstruction, it will be also possible to sample the full integrated luminosity of 200 pb$^{-1}$ for measurements of rare probes over a broad momentum range, such as beauty hadrons, charmonia and jets. For the low-momentum region, these measurements were not possible or very limited in Run 2 (the integrated luminosity for the minimum bias sample was $L_{\mathrm{int}} \approx 0.06$ pb$^{-1}$). The measurements of beauty hadrons and jets would establish a high-precision reference for the corresponding measurements in Pb–Pb collisions (the short pp reference run at the same energy as Pb–Pb is not expected to reach the precision of the Pb–Pb measurements for these low-background signals). They would also enable high-precision QCD studies, like a first direct measurement of the dead-cone effect on gluon radiation off beauty quarks [4], thanks to possibility of measuring jets with a transverse momentum as low as 10–20 GeV/$c$. The measurements of rare charmonium states and of J/$\psi$ production in association with jets and photons, over a rapidity range of 4 units, would provide insight on the charmonium production mechanism and on the proton structure. Central exclusive production of low-mass diffractive states in pp collisions at the LHC serves as a valuable source of information on the non-perturbative aspects of the strong interaction. The increase of integrated luminosity by a factor 20 with respect to Run 2 will also enable the study of the spin structure of the Pomeron and the search of exotic QCD objects, such as glueballs.

– **Study of possible virtual photon production using low-mass dielectrons.** A possible enhancement in the spectrum of low-$p_{\mathrm{T}}$ and low-mass dielecron pairs has recently been reported in pp collisions at $\sqrt{s} = 13$ TeV, using a data sample collected in Run 2 with a reduced value of the ALICE solenoid magnetic field [5]. The reduced field is instrumental for studying this kinematic region, because it largely increases the acceptance for soft dielectrons. The measured enhancement with respect to the expected hadronic sources (dominantly Dalitz decays) could be explained by virtual photon production. A minimum bias sample with an integrated luminosity of about 3 pb$^{-1}$ (300-times larger than that used for the present measurement), which could be recorded in about two weeks, would enable a precise characterisation of this dielectron source, with studies differential in invariant mass, transverse momentum and event multiplicity.

These physics motivations are discussed in Section 2, along with the competitiveness of the proposed ALICE studies with measurements that could be carried out by the other LHC experiments. The following Sections 3 and 4 describe the proposed strategies and required computing resources for data taking,

processing and event selection for the two target samples:

1. A sample with $L_{\rm int} \approx 200$ pb$^{-1}$ with nominal value of the ALICE solenoid magnetic field for which about $1/10^3$ of the collision events will be selected, after calibration and reconstruction, either on the basis of particle multiplicity or of about 10 classes of rare signal candidates. This step of reconstruction and event-selection will be carried out on the O$^2$ computing farm using mostly GPU resources. This sample could be recorded in about 36 months of LHC operation at 35% efficiency with an interaction rate at ALICE of 500 kHz and would result in a final data volume of $\sim 5$ PB after event selection. The specific running plan will be defined on the basis of the final schedule of future LHC Runs.

2. A sample with $L_{\rm int} \approx 3$ pb$^{-1}$ with reduced value of the ALICE solenoid magnetic field for which all interactions would be kept; this sample could be recorded in about 20 days of LHC operation at 35% efficiency with an interaction rate at ALICE of 500 kHz and would result in a final data volume of $\sim 8$ PB.

The additional radiation load resulting from the extended pp operation is reported in Section 5. The total integrated dose would increase by a factor of about four, but it would still be well within the radiation tolerance of the most critical detector components (innermost sensors of the ITS and the MFT). Anyway, after significant radiation exposure via pp and Pb–Pb collisions during the first year, the quality of the full detector response will be assessed to confirm the validity of the anticipated large safety margins (see Section 5).

An assessment of the actual computing resources (determined by the fraction of reconstruction that can be ported to GPUs) could allow us to consider an increase of the interaction rate, in order to reach the integrated luminosity goal already by the end of Run 3.

## 2 Physics motivation

### 2.1 High-multiplicity programme

The discovery of collective phenomena in small collision systems (pp and p–Pb) and of a smooth continuous evolution of particle production with event multiplicity from pp to Pb–Pb collisions has surprised the community at large. Both the measurement of long-range correlation structures (the *ridge*) and the increasing production of strangeness as a function of multiplicity were unexpected and gave rise to a tremendous experimental and theoretical activity in recent years: some of the related publications rank among the highest cited publications of the ALICE, ATLAS and CMS Collaborations [6–8].

These discoveries have challenged two paradigms at once. They have challenged the descriptions explaining phenomena in large heavy-ion collisions and opened the questions *What is the smallest system where they remain valid? Is a QGP formed in proton–proton or proton–lead collisions?* At the same time, the intriguing effects observed in high-multiplicity pp and p–Pb collisions have challenged the standard descriptions used for pp collisions in terms of a (or very few) hard scattering processing and an softer underlying event; *can this description remain standard?* The theoretical explanation and description attempts of the effects observed in small systems span the entire field between fluid dynamics (many scatterings) and the free-streaming limit (no scatterings). Further experimental and theoretical work is needed for a full understanding of the underlying dynamics. While it is evident that the underlying QCD is the same theory, the aim of future experimental and theoretical work is to either demonstrate that a unified description from $e^+e^-$ via pp collisions to Pb–Pb collisions is feasible, or to show that new mechanisms are important in heavy-ion collisions. In other words a single overarching question emerges: *Can there be a consistent understanding of hadronic collisions and particle production across colliding systems, in which a superposition of microscopic QCD processes transitions to a macroscopic QGP?*

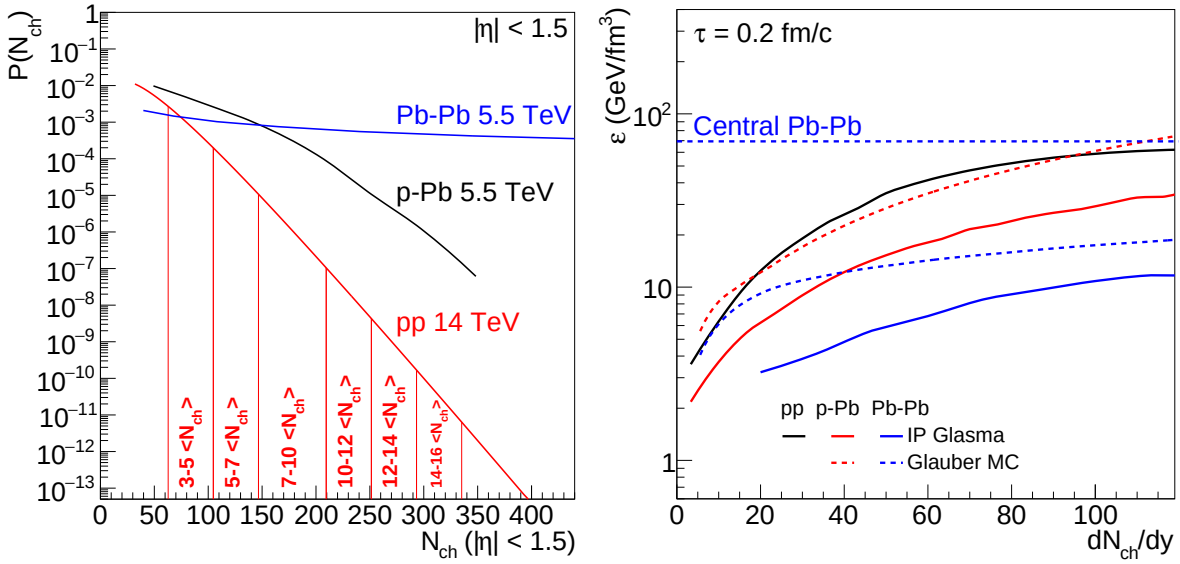


**Fig. 1:** Left: Extrapolated multiplicity distribution in pp collisions within $|\eta| < 1.5$ [3]. The multiplicity distribution of Pb–Pb and p–Pb collisions is also shown. Right: Energy density, averaged over the transverse area, as a function of $\mathrm{d}N_{\mathrm{ch}}/\mathrm{d}y$ calculated by IP-Glasma (solid lines) and with MC Glauber and the Bjorken formula (dashed lines); for details see Ref. [3, Section 9.4.2]. Compared are pp ($\sqrt{s} = 7\,\mathrm{TeV}$), p–Pb ($\sqrt{s_{\mathrm{NN}}} = 5.02\,\mathrm{TeV}$) and Pb–Pb ($\sqrt{s_{\mathrm{NN}}} = 5.02\,\mathrm{TeV}$) collisions at $\tau = 0.2\,\mathrm{fm/c}$. The horizontal line indicates the energy density reached in central Pb–Pb collisions ($\mathrm{d}N_{\mathrm{ch}}/\mathrm{d}y \approx 2000$).

We propose to advance in addressing these questions by inspecting with the upgraded ALICE experiment in Run 3 a sample of high-multiplicity pp collisions with an integrated luminosity of 200 $\mathrm{pb}^{-1}$. On the one hand, this will allow us to extend to higher multiplicity and to make more comprehensive the studies that were started in previous LHC runs. On the other hand, this large sample will enable an extension of the searches for yet-unobserved effects, like jet quenching. This proposal also builds on the studies carried out by the working group on high-density QCD (WG5), with participation from the four large LHC experiments and the theory community, of the 2017–18 HL-LHC workshop [3, Chapter 9].

For the projections in this document a distribution of the number of charged particles extrapolated to very high multiplicity for 14 TeV pp collisions is used which is based on measurements from ALICE data (given that it is an extrapolation, it should only be seen as an educated guess, as discussed in Ref. [3, Section 9.4.1]). Figure 1 (left panel) shows this distribution compared to p–Pb and Pb–Pb collisions. For an integrated luminosity of $200\,\mathrm{pb}^{-1}$, $2.8 \times 10^4$ events are expected with a multiplicity of 14–16 times the average charged particle multiplicity of a pp event ($\langle N_{\mathrm{ch}} \rangle$), i.e. $\mathrm{d}N_{\mathrm{ch}}/\mathrm{d}\eta \approx 100$, which is the same as measured in Pb–Pb collisions with centrality of about 65%. The right panel of Fig. 1 shows an estimate for the energy density that is reached in the different systems, based on the Bjorken estimate (dashed lines) and IP-Glasma (solid lines) [9]. These estimates clearly depend on the assumptions made, in particular for pp and p–Pb collisions, but are used here to illustrate that the energy density depends on the system at a fixed multiplicity, and can reach large values in pp and p–Pb collisions, of the order of the density in central Pb–Pb collisions. In addition, for a given multiplicity, the energy density could be significantly larger in pp with respect to p–Pb collisions, because the transverse overlap area is estimated to be somewhat larger in p–Pb than pp, as confirmed by femtoscopic measurements [10]. The extended multiplicity coverage will also enable more systematic studies of event shapes, already started by ALICE with Run 1 and Run 2 data samples [11, 12]. It has been extensively documented that sphericity, spherocity, as well as other event-shape classification variables, open interesting possibilities to understand the interplay between the production of jets and the underlying events. Recent phenomenological studies have emphasised the importance of studying high-multiplicity events to possibly identify fea-

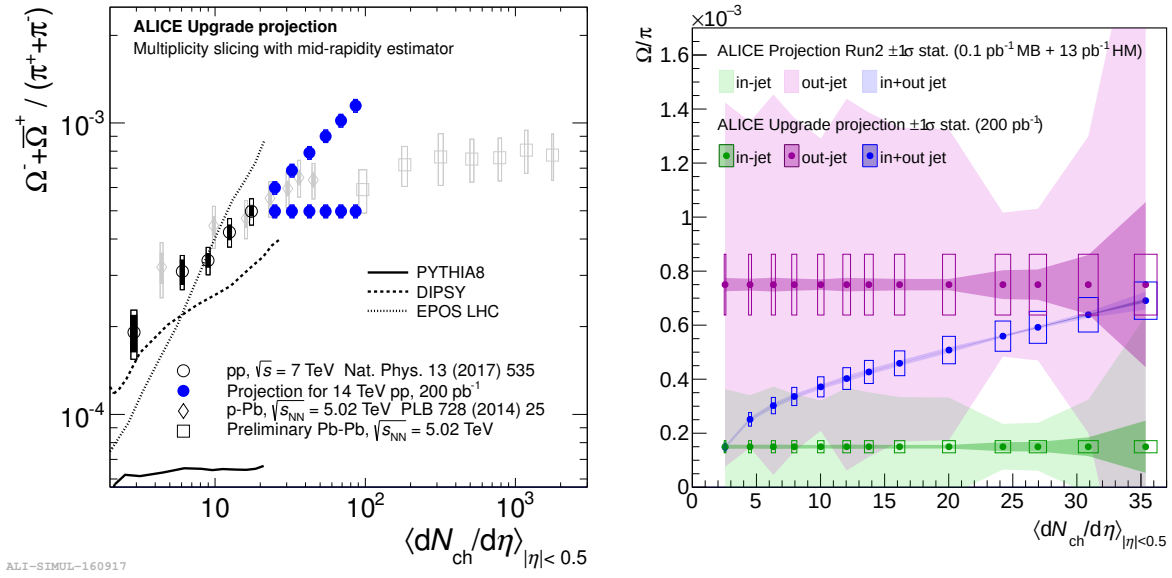


**Fig. 2:** Left: $\Omega/\pi$ ratio as a function of $\mathrm{d}N_{\mathrm{ch}}/\mathrm{d}\eta$ for pp, p–Pb, and Pb–Pb collisions. The existing data (from Ref. [15]) is shown in open black symbols (pp), grey diamonds (p–Pb) and grey squares (Pb–Pb), while the extrapolation for pp collision is shown in blue filled circles. Two scenarios are shown: a) assuming that the ratio continues increasing following the measured trend, and b) assuming that the value saturates at the largest measured $\mathrm{d}N_{\mathrm{ch}}/\mathrm{d}\eta$. Figure from Ref. [2]. Right: $\Omega/\pi$ ratio as a function of the event multiplicity at central rapidity (in event classes based on a forward rapidity estimator). Blue points correspond to inclusive production, purple points to out-of-jet production and green points to in-jet production. The lighter shaded bands correspond to $\pm1\sigma_{\mathrm{stat}}$ projections using the full Run 2 minimum bias and forward-multiplicity-triggered data samples (the narrowing of the band for multiplicity above 20 is due to the presence of the high-multiplicity-triggered sample). The darker shaded bands correspond to projections for $L_{\mathrm{int}} = 200$ pb$^{-1}$. Systematic uncertainties are shown as boxes and provisionally assumed to be the same for the two projections.

tures connected to parameters of a high-density QCD medium, like the degrees of freedom and the sound velocity [13, 14].

In the following, we report the expected multiplicity reach and performance for three representative measurements that would provide insight on three crucial aspects related to the aforementioned questions: a) extending and understanding the strangeness enhancement as a function of multiplicity; b) extending and understanding the dynamics of collective flow using identified hadrons; c) searching for jet-quenching.

**Strangeness production.** The unexpected increase of the strange-particle yield normalized by the pion yield as a function of $N_{\mathrm{ch}}$ is one of the key findings in small systems. In pp collisions these ratios are measured up to $\mathrm{d}N_{\mathrm{ch}}/\mathrm{d}\eta \approx 17$ with 7 TeV data [15] and recently extended to $\approx 22$ with 13 TeV data [16], with some overlap with p–Pb collisions. The most peripheral Pb–Pb collisions measured have a $\mathrm{d}N_{\mathrm{ch}}/\mathrm{d}\eta \approx 96$, nearly 4.5 times larger. In the following, the $\Omega$ baryon is considered for the performance projections because it contains three strange quarks and, thus, it is the most sensitive to the strangeness production and hadronization dynamics. Figure 2 (left) presents the expected reach of the $\Omega/\pi$ ratio measurement in pp collisions which will bridge the present gap between pp and Pb–Pb collisions. If strangeness production reaches the thermal limit in high-multiplicity pp collisions, the $\Omega/\pi$ ratio would level off as a function of multiplicity smoothly connecting with the Pb–Pb results. In another possible scenario in which, for instance, the strangeness enhancement scales with the energy density of the system, it should indeed be possible to see that the high-multiplicity pp results exceed the low multiplicity Pb–Pb results. With the multiplicity reach indicated in Fig. 2 (left), based on a sample of 200 pb$^{-1}$ pp collisions, the two qualitatively different scenarios can be distinguished by the experimental data.

In addition to extending the multiplicity reach with high-multiplicity event selection, as illustrated in the figure, the extended pp programme would also provide a sample of $\sim 10^9$ events selected on the basis of the presence of a reconstructed $\Omega$ baryon. This sample, larger by more than three orders of magnitude than that of Run 2, would enable high-precision multiplicity-differential studies of $\Omega$–jet correlations to separate hard-scattering and underlying-event related $\Omega$ production patterns which could shed light on the microscopic origin of the strangeness enhancement. Several theoretical approaches predict a different strange-to-pion ratio in- and out-of- jets, but in both cases with no multiplicity dependence [17, 18]. The pattern observed in Fig. 2 (left) could then originate from the evolution with multiplicity in the relative contribution of the jet and underlying-event parts to the event. This aspect can be studied by measuring $\Omega$–hadron correlations, selecting regions of the $\Delta\varphi$–$\Delta\eta$ space which are associated with the presence of a jet, and regions which are dominated by particles produced in the underlying event. As an example study, the proxy to define the jet direction is the highest-$p_{\mathrm{T}}$ charged hadron in the event (trigger particle, with at least 3 GeV/$c$ $p_{\mathrm{T}}$). The in-jet region is identified by $|\Delta\varphi| < 1$ rad and $|\Delta\eta| < 0.4$, while the out-of-jet region corresponds to $1 < \Delta\varphi < 2$ rad and $0.5 < \Delta\eta < 1.1$ with respect to the trigger particle. The production yield inside the jet region is also subtracted by the scaled out-of-jet yield, in order to statistically select the genuine jet-related production yield. In Fig. 2 (right), the projection for this study using $L_{\mathrm{int}} = 200$ pb$^{-1}$ is shown. Inclusive (blue), in-jet (green) and out-of-jet (purple) $\Omega$ production are shown. In this study, the multiplicity dependence of $\Omega$ yields in the two regions have been calculated in the hypothesis of multiplicity-independent $\Omega/\pi$ ratio for both components. The very high number of accessible $\Omega$ baryons would allow us to distinguish between in-jet, inclusive and out-of-jet produced $\Omega$ over a large multiplicity range. The projections for the Run 2 minimum bias and forward-multiplicity-triggered data samples show that this measurement is currently out of reach.

**Elliptic flow with multi-particle cumulants and hadron-species dependence.** Long-range multi-particle correlations have been observed in high-multiplicity collisions of protons and protons and nuclei, which suggest that also in these collisions there could be a collective expansion of the collision zone. The key questions are how collective expansion can build up in small collision systems, and whether these phenomena can provide a microscopic picture of hydrodynamic flow. These questions are being actively debated from several viewpoints. These include hydrodynamical models, transport models with hadronic rescattering, rope hadronisation models with string shoving, as well as the colour glass condensate (CGC) effective field theory.

Multi-particle cumulant measurements are a key tool to gain further insight in several collective phenomena in small systems, because, compared to the two-particle correlations, they suppress non-global few-particle correlations (from resonance decays and jets). The projected uncertainties on multi-particle cumulants $v_2\{m\}$ for a high-multiplicity sample of $L_{\mathrm{int}} = 200$ pb$^{-1}$ pp collisions are below 0.007 for $m$ up to 12 (12-particle correlations). These small uncertainties are barely visible in the compilation in Fig. 3 (left). These measurements would overlap in multiplicity with p–Pb and Pb–Pb collisions with sufficient precision to quantify the difference between peripheral Pb–Pb and high-multiplicity pp and p–Pb collisions. The latter comparison would also provide quantitative information about the initial density profile in the two colliding systems: the combination of larger initial energy density in pp and larger initial eccentricity in p–Pb collisions is expected to lead to a distinctive pattern in the flow harmonics in the two systems (see e.g. Ref. [9]).

Measurements of the $p_{\mathrm{T}}$-differential elliptic flow coefficient for identified particles provide additional important information on the origin of flow: a common flow velocity field produces a characteristic mass dependence of the elliptic flow. In pp collisions, the large residual non-flow results in a positive 4-particle cumulant ($c_2\{4\} = -v_2\{4\}^4$) and thus prevents to measure $v_2\{4\}$. This non-flow contamination could be significantly suppressed by using the 3-subevent method, which only allowed us to study of $p_{\mathrm{T}}$-integrated 4-particle cumulants for inclusive charged particles in Run 2 [20]. The large high-multiplicity sample that can be collected in Run 3 will enable $p_{\mathrm{T}}$-differential measurements of identified hadrons using the

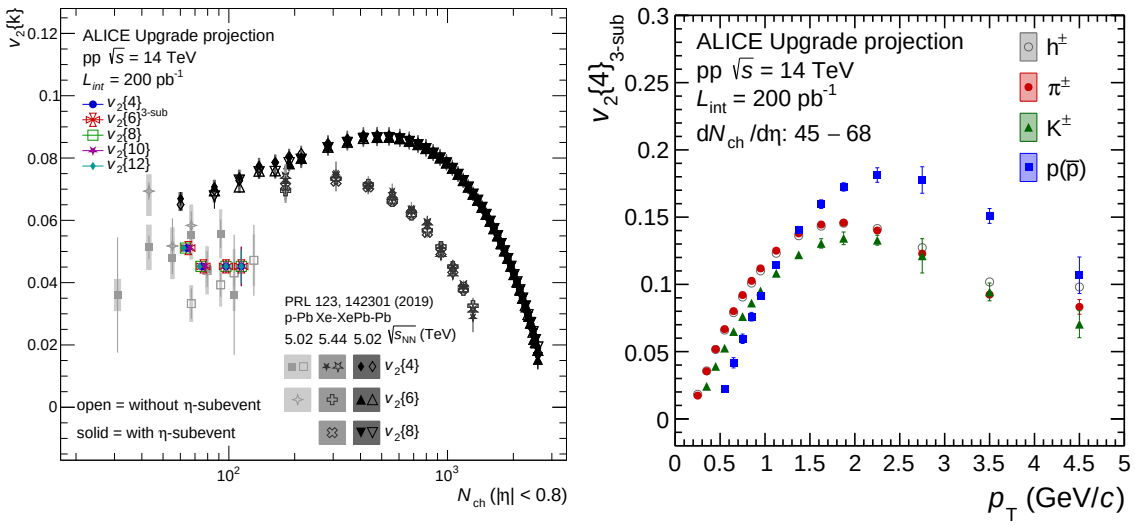


**Fig. 3:** Left: Projected precision of multi-particle cumulant measurements as a function of $N_{\mathrm{ch}}$ for a pp data sample with $L_{\mathrm{int}} = 200$ pb$^{-1}$. The published results in p–Pb, Xe–Xe and Pb–Pb collisions are shown for comparison [19]. Right: Projected $p_{\mathrm{T}}$ differential measurements of $v_2\{4\}_{3-\mathrm{sub}}$ for charged hadrons, $\pi^{\pm}$, K$^{\pm}$, and p($\overline{\mathrm{p}}$) in an event class with $\mathrm{d}N_{\mathrm{ch}}/\mathrm{d}\eta \approx 55$.

3-subevent method. Figure 3 (right) shows the projected performance for events with $\mathrm{d}N_{\mathrm{ch}}/\mathrm{d}\eta \approx 55$, i.e. about 8 times the average multiplicity. An observation of mass ordering at low $p_{\mathrm{T}}$ (0.2–1 GeV/$c$) would provide an unambiguous signal of final-state collective expansion (radial flow) in high-multiplicity pp collisions. A precise comparison of mesons and baryons at higher $p_{\mathrm{T}}$ (2–5 GeV/$c$) would, on the other hand, address the question on whether such collective expansion is built at partonic (constituent quark) level.

**Search for jet quenching.** The measurement of flow phenomena in high multiplicity pp collisions suggests the possible formation of a QGP in small systems. It is therefore natural to search for other effects that, in nucleus–nucleus collisions, are induced by the QGP medium. A prominent effect of this type is jet quenching, which corresponds to the interaction with the QGP of energetic virtual partons generated in hard scattering processes with high squared momentum transfer ($Q^2$). The most well-established signature of jet quenching is energy loss, measured by the suppression of high-$p_{\mathrm{T}}$ hadron or jet yield relative to that in a reference system. The measurement of *inclusive* yield suppression ($R_{\mathrm{AA}}$) requires the scaling of the reference system yield by the geometric factor $N_{\mathrm{coll}}$, which is calculated by associating Event Activity with collision geometry using the Glauber model. However, the association of event activity (EA) with collision geometry is prone to bias in small systems thereby masking the effects of jet quenching [21]. ALICE has developed an alternative approach to jet quenching measurements in small systems, based on the semi-inclusive distribution of recoil jets relative to a high-$p_{\mathrm{T}}$ trigger hadron or photon (as sketched in the left panel of Fig. 4) [22]. By measuring the rate of one hard process relative to another (i.e. number of recoil jets per trigger) the necessity to interpret event activity geometrically is avoided. An initial measurement using this approach has set a limit (90% CL) on medium-induced energy transport out-of-cone in high-EA p–Pb collisions of a factor 20 smaller than that in central Pb–Pb collisions at the LHC [22].

It is clear from these considerations that jet quenching effects in small systems are small. Measuring or setting further limits on their magnitude requires statistical precision significantly beyond currently reported results. Figure 4 (right) shows the measured value of medium-induced energy loss in Pb–Pb collisions, the measured limit in p–Pb collisions, and the projected limits for pp and p–Pb collisions in Run 3 [2]. ALICE measurements based on high-multiplicity-selected pp collisions with $L_{\mathrm{int}} = 200$ pb$^{-1}$

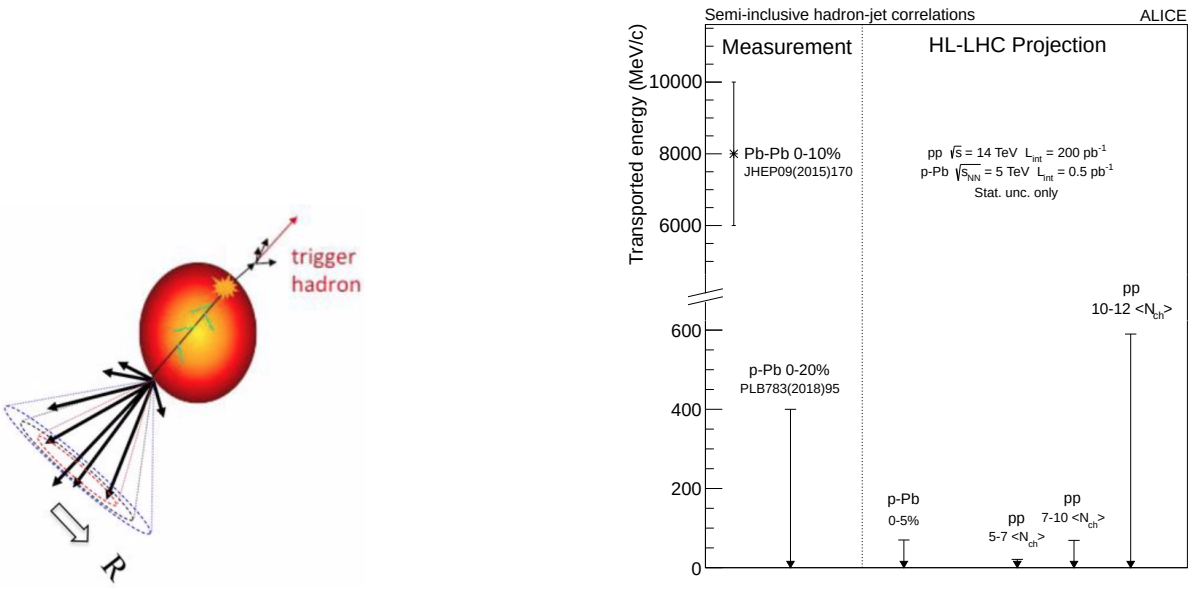


**Fig. 4:** Projection of semi-inclusive hadron–jet measurements (sketch in the left panel) of jet quenching for high-multiplicity-selected pp collisions with $L_{\rm int} = 200$ pb$^{-1}$ and p–Pb collisions in LHC Run 3 [2, 3]. The figure shows the projected sensitivity to the minimum jet spectrum shift (transported energy) with 90% confidence level, in comparison to the measurement and limit in Pb–Pb and p–Pb collisions from Runs 1 and 2 [22].

will clearly provide a significant improvement in the measurement of jet yield suppression and either identify or set stringent limits on effects due to jet quenching. For example, both the pp class with multiplicity 7–10 times the average multiplicity and the p–Pb class with 0–5% EA could be sensitive to a transported energy as low as 70 MeV, allowing us to precisely compare possible effects in systems with similar multiplicity, but different sizes (larger in p–Pb) and energy densities (larger in pp).

ALICE has recently also explored di-jet acoplanarity as a signature of jet quenching in high-multiplicity pp collisions at $\sqrt{s} = 13$ TeV, using a high-multiplicity online trigger that inspected a total integrated luminosity of 13 pb$^{-1}$. This dataset enables a statistically-significant acoplanarity measurement for event multiplicity corresponding to about 5 times the mean multiplicity. While this preliminary analysis is still under active study, it is clear that sampling 200 pb$^{-1}$ in Run 3 will provide much higher precision and a broader range in multiplicity. This rich dataset will provide high discriminating power to separate initial and final-state effects on acoplanarity distributions and other related distributions affected by potential jet quenching. In addition to high-multiplicity events, the selection after reconstruction would also provide a large sample in which a jet recoils against a high-energy photon (measured in the PHOS or EMCal detectors). This sample will enable studies of acoplanarity and recoil yield suppression with a better di-jet axis resolution and without potential quenching of the trigger particle in the above mentioned semi-inclusive studies.

### 2.2 Light (hyper-)nuclei production and hadron–hadron interactions

**Nuclei and hyper-nuclei.** The study of anti- and hyper-nuclei in pp collisions at the LHC is mainly motivated by the following two goals:

– The production cross sections of $^3\overline{\rm He}$ and $^4\overline{\rm He}$ in pp collisions provide crucial input for the indirect searches of Dark Matter with cosmic rays by AMS-02 [23] and GAPS [24] collaborations, because Dark Matter candidates are predicted to annihilate into nucleus–antinucleus pairs. However, the production of nuclei and antinuclei in ordinary proton–proton and proton–nucleus collisions in Space represents a large, poorly known, background for these searches. In this context, the measurements in pp collisions are more relevant than those in nucleus–nucleus and proton–nucleus

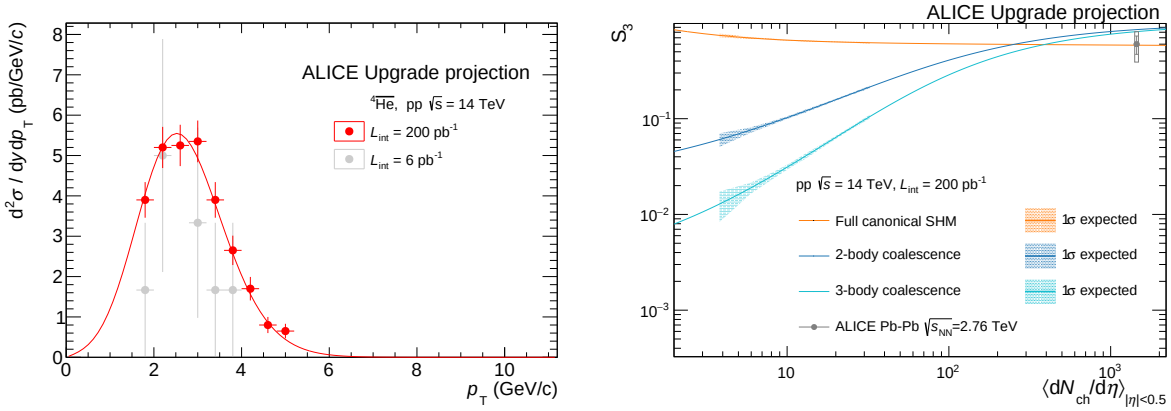


**Fig. 5:** Left: Expected $^4\overline{\text{He}}$ $p_{\text{T}}$-differential cross section as a function of $p_{\text{T}}$. The red points represent the expected statistical precision for a sample corresponding to $L_{\text{int}} = 200$ pb$^{-1}$, while the grey points assume the integrated luminosity of the dedicated pp run at $\sqrt{s} = 5$ TeV. Note that the cross section is the same also for nuclei. Right: $S_3$ measured from hyper-triton production as a function of multiplicity compared with three production models [28, 29]; the measurement in Pb–Pb collisions is shown [30] together with projected precision for measurements in pp collisions with $L_{\text{int}} = 200$ pb$^{-1}$.

collisions because the Universe consists mostly of hydrogen. The measurement of $^4\overline{\text{He}}$ is of particular importance in this context as the preliminary ratio of $^4\overline{\text{He}}$ to $^3\overline{\text{He}}$ poses a challenge for the dark matter astrophysics community (see for instance the discussion in [25]).

– In order to distinguish different production scenarios for light nuclei and hyper-nuclei (thermal statistical production or coalescence of nucleons), small collision systems, like pp collisions, are advantageous, because the coalescence probability is expected to depend on the size of the produced nucleus with respect to the size of the particle emitting source.

The study of nuclei and hyper-nuclei requires a large integrate luminosity, given that their production yield decreases by a factor of about 1000 for each additional nucleon [26]. First estimates on the expected uncertainties for the coalescence parameters $B_3$ (A = 3) and $B_4$ (A = 4) were obtained for the HL-LHC CERN Yellow Report [3]. There it has been outlined that a $O(10\%)$ precision is required for astrophysical applications. For $B_3$, such a precision is already achievable in $L_{\text{int}} = 6$ pb$^{-1}$ in pp collisions at $\sqrt{s} = 5.5$ TeV. A first measurement of several $^4\overline{\text{He}}$ candidates might be achievable in the same data sample. However, a statistical precision on $B_4$ at $O(10\%)$ level in 4 to 5 $p_{\text{T}}$ intervals will require a larger $L_{\text{int}} = 200$ pb$^{-1}$ data sample at $\sqrt{s} = 14$ TeV as shown in Fig. 5 (left). These expectations are based on the exponential fit of the existing measurements of the d$N$/d$y$ of $\overline{\text{d}}$, $\overline{\text{t}}$, and $^3\overline{\text{He}}$ in pp collisions at $\sqrt{s} = 7$ TeV [26], which are extrapolated to $\sqrt{s} = 14$ TeV by a scaling of the corresponding d$N$/d$\eta$ values and the inelastic pp cross sections from [27]. Such a large integrated luminosity can be inspected with a dedicated event selection on the TPC specific energy loss for nuclei. This would be the first observation ever of the $^4\overline{\text{He}}$ nucleus in pp collisions.

For the study of production scenarios, the most promising probe is provided by the study of the hyper-triton $^3_\Lambda$H (a bound state of a proton, a neutron and a $\Lambda$). In coalescence models, its production is largely suppressed due its wide wave-function. This effect is largest in pp collisions and less pronounced in Pb–Pb collisions, as it is the relative difference between the system size and the size of the produced object that matters. In thermal-statistical models, such suppression of large objects is not present. However, the explicit conservation of baryon and strangeness number may lead to the suppression of nuclei and hyper-nuclei in small systems. In order to cancel out these effects, the so-called $S_3$ variable is defined by

combining the production yields of ${}^{3}_{\Lambda}\mathrm{H}$, ${}^{3}\mathrm{He}$, $\Lambda$ and protons as

$$S_3 = \frac{{}^{3}_{\Lambda}\mathrm{H}/{}^{3}\mathrm{He}}{\Lambda/\mathrm{p}} \,. \tag{1}$$

As shown in Fig. 5 (right), this ratio is expected to be around 0.6 in thermal-statistical models [29] with only a mild increase towards small systems, while in coalescence models [28, 31] it exhibits a dramatic drop towards smaller multiplicities due to the wide wave-function of the hyper-triton. Thus, a precise measurement of $S_3$ in small collision systems will provide a large sensitivity to distinguish these two production scenarios.

**Proton–hyperon and hyperon–hyperon interaction via correlation measurements.** The study of two-particle correlations in momentum space measured in ultra-relativistic pp and p–Pb collisions has proven to provide direct access to the interaction between rare particle pairs in vacuum [20, 32–36]. In particular due to the small size of the colliding systems of about 1 fm, the resulting pronounced correlation signal from strong final state interactions allows for detailed studies of the latter, and hence provides additional data with unprecedented precision in the low momentum regime.

High-multiplicity pp collisions present a suitable environment to study correlations because the pair production rate in such collisions is significantly larger than in minimum bias collisions. For example, a five-fold increase in particle pairs per event is expected for the high-multiplicity data sample with $N_{\mathrm{ch}} > 7\ \langle N_{\mathrm{ch}} \rangle$ that can be collected in Run 3 with respect to the high-multiplicity sample that was recorded in Run 2. This and the increase by a factor larger than 10 of the integrated luminosity will increase the yields by a factor larger than 50.

In contrast to the nucleon–$\Lambda$ (N–$\Lambda$) interaction, the nature of the N–$\Sigma$ interaction still lacks conclusive and firm experimental constraints. Indeed, experimental measurements from scattering data [37], hypernuclei production data [38, 39] and $\Sigma^-$ atomic data [40, 41] are available, but are not very precise or conclusive. Recent results point towards an attractive interaction in the isospin $I = 1/2$ channel of the N–$\Sigma$ system [38], and repulsion in the $I = 3/2$ channel [39] with, however, a substantial model-dependence in the interpretation. The measurement of the p–$\Sigma^0$ correlation function in high-multiplicity pp collisions by ALICE demonstrated the feasibility of the approach [20]; however, the current results have large statistical uncertainties and relatively low signal purity, meaning that no final conclusion can yet be drawn for this interaction. The reconstruction of the $\Sigma^0 \to \Lambda\gamma$ decay is rather challenging due to low energy of the photon, which significantly affects the efficiency of the measurement. The left panel of Fig. 6 shows the correlation function with statistical uncertainties scaled according to the expected high-multiplicity pp data sample at $\sqrt{s} = 14$ TeV. The precision of the measurement at reduced relative momentum of the pair $k^* = 40\,\mathrm{MeV}/c$ will be about 4% in $50\,\mathrm{MeV}/c$ wide bins. The projection is obtained on the basis of the ESC16 model [42], which provides the best agreement with the presently measured correlation function [20]. In particular in the N–$\Sigma$ sector, the profile of the modelled correlation function is sensitive to details of the strong interaction. Therefore, the reduced statistical uncertainties of the p–$\Sigma^0$ correlation function in pp collisions at $\sqrt{s} = 14$ TeV will contribute to an improved understanding of the interaction.

The HAL-QCD method has been used as well to perform Lattice QCD calculations at the physical point for the $\Omega$–$\Omega$ system, where the most strange dibaryon ($S = 6$) has been predicted [44] with a binding energy of about 1.6 MeV. This is implied by the attractive character of the $\Omega$–$\Omega$ strong interaction and the fact that the Pauli principle does not apply for this system. The measurement of the $\Omega$–$\Omega$ correlation function is extremely challenging and has not been possible to date. With an expected raw yield of $1.6 \times 10^{-4}$ $\Omega^-$ or $\Omega^+$ per event within the ALICE central barrel acceptance, an event selection for $\Omega$ decays could be set up to sample the whole $200\,\mathrm{pb}^{-1}$ of pp collisions at $\sqrt{s} = 14$ TeV in Run 3, resulting in a total of $2 \times 10^9$ recorded $\Omega^-$ or $\Omega^+$. In this sample, about 500 $\Omega$–$\Omega$ pairs are expected with low relative momentum, $k^* < 200\,\mathrm{MeV}/c$. Hence, a precision in the correlation function similar to the one obtained for the current p–$\Omega$ Run 2 analysis is expected with the Run 3 data: 30% at $k^* = 50\,\mathrm{MeV}/c$ with

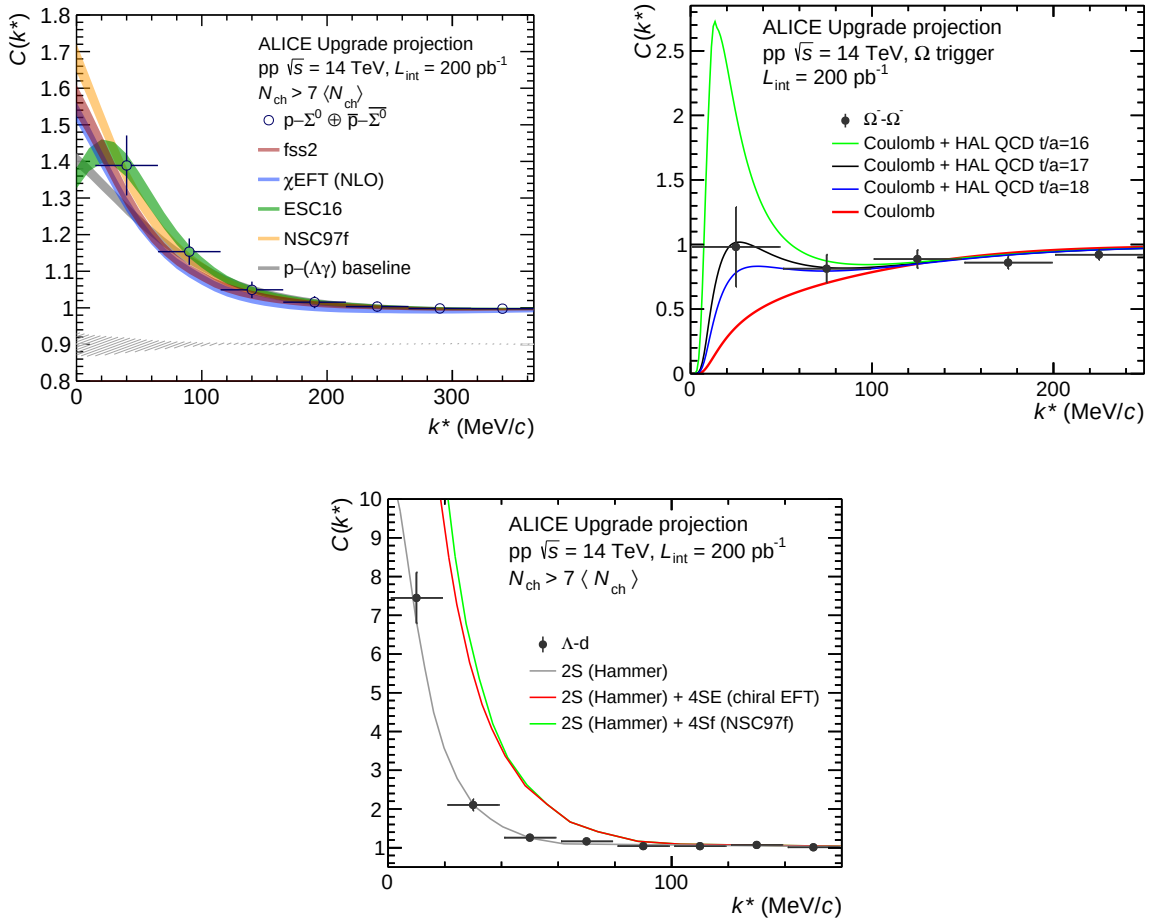


**Fig. 6:** Upper left: Projected p–$\Sigma^0$ correlation function for the $L_{\rm int} = 200\,{\rm pb}^{-1}$ pp data sample at $\sqrt{s} = 14$ TeV with different model predictions [42, 43]. Only the scaled statistical uncertainties are shown. The dashed area denotes the correlated uncertainty due to the modeling of the p–$(\Lambda\gamma)$ baseline which is substantially reduced due to the enhanced data sample and the improved efficiency. Upper right: Expected precision of the Ω–Ω correlation function, simulated following the Coulomb + strong (HAL QCD, $t/a = 17$) interaction, for the $L_{\rm int} = 200\,{\rm pb}^{-1}$ pp data sample at $\sqrt{s} = 14$ TeV using a dedicated Ω-decay event selection. The correlation function obtained with the inclusion of the HAL-QCD strong potential with different integration times $t/a$ are also shown with coloured lines [44]. Lower panel: projected Λ–d correlation function for the $L_{\rm int} = 200\,{\rm pb}^{-1}$ pp data sample at $\sqrt{s} = 14$ TeV with different model predictions [45], only statistical uncertainties are shown.

a bin width of 50 MeV/$c$. In Fig. 6 (upper right), a projection of this measurement is shown, which would represent a first-ever assessment of the Ω–Ω strong interaction and would be sensitive to the details of the strong potential (three versions of the HAL QCD potential for a source radius of $r = 0.80$ fm [44]).

Additional studies will be carried out using the pp high-multiplicity-selected event sample from Run 3, taking advantage of the enhanced strangeness production. For instance, the correlation analysis of p–$\Xi^0$ pairs will become possible, complementing the existing p–$\Xi^-$ measurement [33, 36]. The precision in the p–Ω analysis [36] could be improved by orders of magnitude, so that the compatibility of the data with the models predicting the formation of a N–Ω bound state [46, 47] could be effectively tested in the region around $k^* = 150$ MeV/$c$. In this region, a characteristic depletion of the correlation function below unity at the percent level is predicted as a sign of the formation of the bound state. In addition, thanks to the high-multiplicity-selected sample, it will be possible to constrain the isospin-dependent component of the K–N interaction by studying in detail the $\mathrm{K}^{\pm}$–deuteron correlation function.

Finally, the three body forces involving hyperons and nucleons, that are extremely important for the understanding of the structure of neutron stars [48], can be investigated measuring baryon-nucleus correlations. An example of this kind of measurements is the study of the correlations between (anti)Λ hyperons and (anti)deuterons. While there are no Λ–deuteron scattering measurements, in the current theoretical frameworks the lower spin component ($^2S_{1/2}$) of this interaction is constrained by the measurements of the hypertriton binding energy. However, higher spin configurations of this interaction are not binding and cannot be investigated with studies on hypernuclei. As shown in the lower panel of Fig. 6, using the high multiplicity selection, it will be possible with 200 $\mathrm{pb}^{-1}$ of pp collisions at $\sqrt{s} = 14$ TeV to measure precisely the deuteron–Λ interaction, complementing the hypertriton binding energy measurements by constraining all the spin components of the interaction [45]. Furthermore, it has been suggested that the study of Λ–deuteron can help in the detailed understanding of coalescence processes [49], complementing the direct $S_3$ measurement mentioned above.

### 2.3 Heavy quarks, quarkonia, jets, diffraction

The possibility to select pp events after full reconstruction opens a broad range of measurements of rare QCD processes, involving heavy-flavour hadrons, quarkonia, jets, photons and central exclusive diffraction. These measurements offer unique insight in several aspects of perturbative and non-perturbative QCD, and, in addition, they will provide us with crucial pp reference measurements for the programme in Pb–Pb collisions.

**Heavy flavour and jets.** The precise measurement of beauty-hadron production in pp collisions down to zero transverse momentum is essential for a precise estimate of the total beauty production cross section, and to provide a precise reference for the measurements of the B-meson nuclear modification factor $R_{\mathrm{AA}}$ in Pb–Pb collisions. As described in Refs. [3, 50, 51], the production yield of $\mathrm{B}^+$ and $\mathrm{B}^0$ mesons will be measured in central Pb–Pb collisions in Runs 3 and 4 with an expected statistical precision, for $L_{\mathrm{int}} = 10$ $\mathrm{nb}^{-1}$, better than 20–25% down to a transverse momentum of 2–3 GeV/$c$, using the $\mathrm{D}^0\pi^+$ and $\mathrm{J}/\psi\mathrm{K}^+$ decay channels for $\mathrm{B}^+$ and the $\mathrm{D}^{*,+}\pi^-$ decay channel for $\mathrm{B}^0$. The integrated luminosity for pp reference runs at the same energy as Pb–Pb collisions is expected to be sufficient for the reference measurements for $\mathrm{B}^+ \to \mathrm{J}/\psi\mathrm{K}^+$, but not for the other decay channels. For the latter, measurements in pp collisions at top LHC energy can be used to define a pp reference for $R_{\mathrm{AA}}$, also considering that the B production cross section is well-described by pQCD calculations (e.g. FONLL [52]), which can thus be used to scale, with small additional theoretical uncertainties, the measured cross section from top LHC energy to the energy of Pb–Pb collisions (see Refs. [50, 51]).

The possibility to reconstruct B-meson hadronic decay channels involving open-charm hadrons and to select pp events in Run 3 on the basis of the presence of a B candidate was studied using full simulations of the upgraded detector and considering the production cross sections predicted by FONLL calculations [52, 53]. Both the signal and the combinatorial background were simulated with the PYTHIA

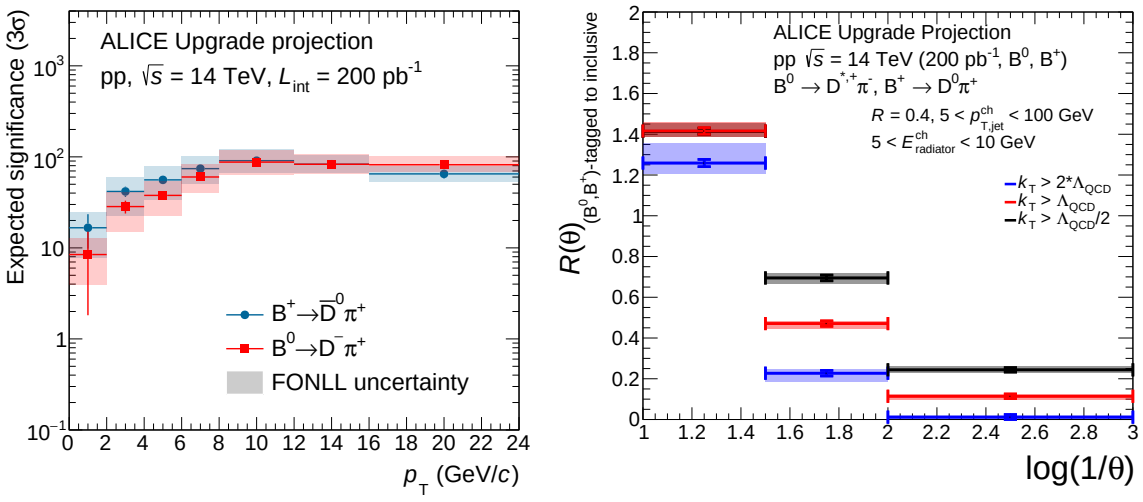


**Fig. 7:** Left: Expected statistical significance for the measurements of $B^+$ and $B^0$ mesons in pp collisions at $\sqrt{s} = 14$ TeV as a function of $p_T$ for $L_{int} = 200$ pb$^{-1}$. Right: Ratio of splitting angle $\theta$ distributions for B-tagged jets and inclusive jet as a function of $\log(1/\theta)$ for jet $5 < p_T < 100$ GeV/$c$, parton radiator energies in the range 5–10 GeV and three threshold values for the transverse momentum of the splittings $k_T$ in units of $\Lambda_{QCD}$ ($= 200$ MeV).

6.4.25 [54] event generator. Figure 7 (left) shows the expected significance for the measurement of the $B^+$ and $B^0$ mesons as a function of $p_T$ for $L_{int} = 200$ pb$^{-1}$. The statistical significance is expected to be of the order of 20 (10) for $B^+$ ($B^0$) mesons with $0 < p_T < 2$ GeV/$c$ and larger than 40 above 2 GeV/$c$. As discussed in Section 3, events with a B candidate with $p_T > 0$ can be selected after full reconstruction with a large rejection factor for events without signal.

Besides the search for jet quenching at high multiplicity, jet and photon triggers are interesting to perform perturbative QCD measurements. With an integrated luminosity $L_{int} = 200$ pb$^{-1}$, the number of jets at $p_T^{jet} = 100$ GeV/$c$ will be of the order of $10^6$, which is sufficient to perform a rich selection of substructure measurements. The combined request of a photon and a jet in event selection after reconstruction will allow us to also keep events with a much lower jet $p_T$ and to study the substructure of quark-initiated jets.

The event sample selected with a B-meson candidate will be used to carry out the jet substructure analysis that was recently pioneered with D mesons and jets to directly observe for the first time the dead-cone effect at hadronic colliders as proposed in [4]. This effect is a manifestation of the reduced probability of gluon radiation off a heavy quark at angles smaller than the ratio of the quark mass over its energy. The analysis used a new technique, based on the iterative declustering of the heavy-flavour-tagged jets, which allows to penetrate the jet shower and access the deepest levels of the clustering history that correspond to the splittings at the smallest angles in an angular-ordered shower. Only the large integrated luminosity of the Run 3 sample and the strong ALICE capabilities for low-momentum jet and B-meson measurements will enable a first measurement of the effect for b quarks. Figure 7 (right) shows the ratio of the distributions of the splitting angle $\theta$ for B-tagged jets and inclusive jets. The B-tagged distribution in the numerator is obtained from PYTHIA8 [55] simulations with the statistical uncertainties based on the $B^0$ and $B^+$ significance in the left panel of the same figure. The strong expected reduction of the ratio below unity at a small angle (large $\log(1/\theta)$) would be a first spectacular direct measurement of the dead cone effect for b quarks. This measurement, among others, will extend the versatility of ALICE and the LHC as a complete QCD laboratory.

A sample of jet triggers corresponding to an integrated luminosity of 200 pb$^{-1}$ would also allow us to

carry out reference measurements of jet substructure with statistical uncertainties comparable to those expected for a sample of Pb–Pb collisions with $L_{\rm int} = 10$ nb$^{-1}$ (the equivalent nucleon–nucleon integrated luminosity of Pb–Pb collisions with $L_{\rm int} = 10$ nb$^{-1}$ is about 400 pb$^{-1}$). Such high-statistics reference measurements would be crucial for the interpretation of the modifications studied in Pb–Pb, although the different centre-of-mass energy will require a validation of the pp reference with detailed event generator benchmarks.

**Charmonium production.** The quantitative understanding of quarkonium production in hadronic collisions remains challenging to state-of-the-art perturbative QCD calculations. In addition to its intrinsic interest, such a more thorough understanding would put on a more robust footing all studies of quarkonium as a probe of deconfined matter. During Run 1 and Run 2, high-precision quarkonium production studies with ALICE were possible with the forward Muon Spectrometer only, and without separation of prompt and non-prompt (feed-down from B decays) components. In Run 3, the event selection after reconstruction will provide the same full integrated luminosity to both measurements at forward rapidity and at central rapidity (di-electron decay channel). The ITS and MFT will enable separating the prompt and non-prompt components in both acceptance regions. Moreover, long-range correlation studies over up to 5 units in rapidity will be possible because both the Muon Spectrometer and central barrel data will be available for each selected event, at variance with separate readout streams that operated in Runs 1 and 2. All these changes will open several relevant physics cases, some unique to ALICE, and some where ALICE can provide the most competitive results.

For the Muon Spectrometer the event selection strategy would rely on the presence of a dimuon with invariant mass larger than 2 GeV/$c^2$. For the central barrel the event selection would be based on the presence of a dielectron pair (J/$\psi$ candidate) with invariant mass in the range 2.6–3.2 GeV/$c^2$ and with each electron having $p_{\rm T} > 1$ GeV/$c$. Both selections would have very large rejection factors (see Section 3) and they would enable a wide range of measurements, including direct J/$\psi$ (spectra, polarization), higher mass charmonium decaying via J/$\psi$ (e.g. $\psi$(2S) and $\chi_{\rm c}$ states), inclusive beauty production via non-prompt J/$\psi$, B mesons via exclusive decay channels, J/$\psi$-jet substructure, exotic states (e.g. X(3872)), and J/$\psi$ production in Double Parton Scatterings (DPS) via double J/$\psi$ or J/$\psi$ production associated with D mesons.

In the following, the estimated reach for these measurements with $L_{\rm int} = 200$ pb$^{-1}$ is presented, considering the central rapidity case for illustration.

- The total number of selected J/$\psi$ mesons will be about $3 \times 10^7$, resulting in a precise production cross section measurement up to $p_{\rm T} = 30$–$50$ GeV/$c$ (about 5 (10)% statistical uncertainties at 30 (50) GeV/$c$) and a precise polarisation measurement up to 20 GeV/$c$.

- The number of reconstructed $\chi_{\rm c} \rightarrow {\rm J}/\psi\gamma \rightarrow {\rm e}^+{\rm e}^-{\rm e}^+{\rm e}^-$ will be about $5 \times 10^4$ allowing the first measurement down to zero $p_{\rm T}$ at central rapidity, which would complement the forward rapidity measurement by the LHCb Collaboration [56].

- The number of reconstructed ${\rm X}(3872) \rightarrow {\rm J}/\psi + \pi^+ + \pi^-$ decays is expected to be approximately 1500 for $p_{\rm T} > 10$ GeV/$c$ (the range covered by the measurement by the CMS Collaboration [57]). There are also good prospects for extending the measurement below 10 GeV/$c$, but a full assessment requires detailed studies that are currently ongoing.

With the foreseen high-multiplicity selection, the multiplicity coverage for J/$\psi$ measurements will be extended from approximately 7 $\langle N_{\rm ch} \rangle$ to 11–13 $\langle N_{\rm ch} \rangle$. The $\psi$(2S) measurements can be carried out with good statistical precision up to 5–8 $\langle N_{\rm ch} \rangle$, which will allow us to search for potential charmonium suppression effects in high-multiplicity events. Additionally, J/$\psi$–hadron correlations will be accessible with high precision. This will enable studies of both short-range correlations, relevant for the produc-

tion mechanism, and long-range correlations, which are sensitive to possible collective effects for charm quarks.

In addition, the associated production of a $J/\psi$ and a photon or a D meson can provide a novel insight on the partonic structure of the proton. The experiments at the HERA accelerator and numerous fixed-target experiments delivered precision data for the partonic structure of protons. Most of these data, however, only provide one-dimensional information on the proton structure, namely the momentum fraction $x$ carried by a given parton. The programme to characterise the proton wave-function in more dimensions, both in transverse coordinate and in momentum space, has progressed significantly, but remains challenging. The back-to-back production of $\gamma + J/\psi$ has been proposed as a tool to probe the gluon transverse momentum dependent parton distribution functions [58]. In this context, the low-momentum coverage of ALICE for both the charmonium and the photon, below the trigger thresholds of ATLAS and CMS, are particularly interesting. Based on the calculations in Ref. [58], about 200 $\gamma + J/\psi$ candidates with $J/\psi$ $p_{\rm T} > 5$ GeV/$c$, $|y| < 0.5$, and no explicit selection on the $\gamma$ $p_{\rm T}$ (the $J/\psi$ creates a hard photon spectrum) are expected in a data sample of pp collisions with $L_{\rm int} = 200$ pb$^{-1}$. This programme is also feasible in LHCb, but in a complementary Bjorken-$x$ range. Another perspective to investigate the proton structure is the study of double or multiparton interactions, i.e. to investigate conditional probabilities for finding several hard scatterings. First results have been obtained by LHCb in the charm sector [59]. ALICE can provide similar measurements at midrapidity, but also by combining the information of the mid- and forward rapidity detectors. The estimated yields are of the order of one to a few hundred for $J/\psi$–$J/\psi$ and $J/\psi$–D, for $L_{\rm int} = 200$ pb$^{-1}$.

**Central exclusive production in diffractive collisions.** Central exclusive production (CEP) of low-mass diffractive states (below the $J/\psi$ mass) in pp collisions at the LHC may serve as a valuable source of information on the non-perturbative aspects of strong interaction. At low masses, CEP is usually described in terms of a double Pomeron exchange (DPE) mechanism. DPE is expected to be an ideal process for the investigation of meson resonances with $I^G(J^{PC}) = 0^+(0^{++}, 2^{++}, \dots)$ quantum numbers and gluonic bound states. Glueball searches in CEP are of particular interest because lattice QCD calculations predict the lightest glueballs to have masses $M_G(0^{++}) = 1710$ MeV and $M_G(2^{++}) = 2390$ MeV [60, 61]. Pure glueballs are predicted to decay equally well into pairs of pions, kaons or $\eta$ mesons with suppressed two photon decays. However, this simple signature is contaminated by the fact that glueballs are expected to mix with nearby $q\bar{q}$ states. Central-exclusive production of low-mass resonances in the $\pi\pi$ and KK channels has been extensively studied in fixed target experiments (see review in [62]) and collider experiments at RHIC [63], Tevatron [64] and the LHC [65]. There is a clear evidence of supernumerous light scalar meson states, not fitting well into the conventional groundstate $q\bar{q}$ nonet and suggesting that some of these states, e.g. $f_0(1370)$, $f_0(1500)$ and $f_0(1710)$ mesons, have a significant gluonic component, but the nature of all these states is still controversial [66]. Higher-precision measurements from the LHC would provide additional important insight.

CEP can be also used to investigate the spin structure of the Pomeron and its coupling to hadrons. The Pomeron is generally thought to represent the absorptive part of the cross section, so it should have the quantum numbers of the vacuum, $J^{PC} = 0^{++}$ [67]. It is also supported by gluon ladder calculations. This assignment gives a natural explanation why s-channel helicity conservation holds in photoproduction, as was seen by a large body of HERA data [68]; it also explains much UPC data. It is, however, disfavored by recent measurements on the helicity structure of small-t proton–proton high-energy elastic scattering from the STAR experiment [69]. Vector and tensor Pomerons have also been discussed in the literature. The vector Pomeron model has problems from the point of view of a field theory. Taken literally, the vector Pomeron model predicts opposite signs for pp and $p\bar{p}$ cross sections [70]. On the other hand, the tensor Pomeron model [71] was found to be perfectly consistent with the STAR data [69, 70]. In contrast to the scalar and vector Pomeron assumption, the tensor model also predicts the production of vector mesons in CEP with quantum numbers $J^{PC} = 1^{--}$.

Measurements of CEP processes rely on the selection of events with only few tracks in an otherwise empty detector. Therefore, large pseudorapidity coverage and low pileup conditions are essential to guarantee the event emptiness. The ALICE detector nicely matches these requirements. First CEP measurements were performed by ALICE in the LHC Run 1 and 2 using an integrated luminosity of about 8 $\text{pb}^{-1}$. During Run 3, data taking with continuous readout mode will guarantee that the full target luminosity of 200 $\text{pb}^{-1}$ can be inspected to select CEP events for the aforementioned glueball searches and Pomeron characterisation. The expected high integrated luminosity will also allow us to open up new channels with respect to Run 2 and measure the spectrum of heavy quarkonium states, e.g. at least $5 \times 10^4$ $\chi_{c0} \to \pi^+\pi^-$ decays are expected in CEP events based on cross section estimates from SUPERCHIC generator [72].

In addition, measurements of open and hidden heavy flavour in photoproduction processes will be possible. Photoproduction of open charm and bottom is of great interest as a theoretically clean way to measure gluon distribution functions at low Bjorken-$x$ [73, 74]. The LHC provides higher photon energies than HERA did, giving access to smaller $x$ values. The presence of a rapidity gap can be used to separate photoproduction from other channels. Photoproduction of heavy quarkonium is experimentally much cleaner than open heavy flavor [75] and it also probes gluon distributions, albeit with larger theoretical uncertainty than the open heavy flavor. Quarkonium production in pp collisions probes the same distributions as in proton–nucleus, since the latter is dominated by proton-target interactions. However, the systematic uncertainties are different, providing an important check, especially at midrapidity, where there is no ambiguity regarding photon energy.

### 2.4 Low-mass and low-momentum dileptons

The enhanced strangeness production and the possible onset of collectivity in pp collisions suggest intense rescattering of the constituents during an intermediate stage of the reaction. As discussed in Section 2.1, this is in contrast to the standard description of pp collisions, where particle production is assumed to occur “in vacuum", i.e., in the absence of an interacting medium. Further insight can be gained from the study of electromagnetic radiation. In an interacting system of charged constituents, real and virtual photons are emitted and, due to their penetrating nature, are expected to leave the system without any further interaction. Photons and dileptons are therefore most valuable probes to investigate the pre-equilibrium dynamics in pp collisions.

The presence of soft photon and dilepton radiation in small collision systems was reported by several fixed-target and collider experiments in the SPS and ISR energy range (see references in Ref. [5]). The measured yields are in excess of expectations from known hadronic sources, including bremsstrahlung off in- and outgoing hadrons, and gave rise to speculations about the existence of an intermediate stage, possessing considerable interaction of constituents. However, no final conclusion could be drawn on this issue, also due to partially contradicting experimental findings. In the past decade, several measurements of low-mass dielectron production in pp collisions at RHIC and at the LHC were reported. All measurements are consistent with the expectations from hadronic decays and reveal no indication for any significant dielectron excess in pp collisions. On the other hand, the typical low-$p_{\text{T}}$ threshold of 0.2 GeV/$c$ for the detection of electrons in such analyses prevents access to the kinematic region of interest at low invariant mass $m_{\text{ee}}$ and pair transverse momentum $p_{\text{T,ee}}$, where medium effects are expected to be most pronounced. Major progress in this direction therefore requires to enhance significantly the experimental sensitivity for electrons with $p_{\text{T}} < 0.1$ GeV/$c$.

Owing to its low material budget and its superior tracking, vertexing and PID capabilities at low $p_{\text{T}}$, the ALICE detector is ideally suited for the measurement of soft dielectrons at midrapidity. Another important experimental aspect was excercised in special campaigns during pp operation in Run 2 at $\sqrt{s} = 13$ TeV, where the magnetic solenoid field in the ALICE central barrel was reduced from 0.5 to 0.2 T and a data sample of about 9 $\text{nb}^{-1}$ was collected. In this magnetic-field configuration, the

single-electron low-$p_{\mathrm{T}}$ detection threshold could be reduced to 0.075 GeV/$c$, which makes possible the reconstruction of dielectron pairs with vanishing pair transverse momentum down to invariant masses of 0.15 GeV/$c$. This sensitivity to soft (di)electrons is unique at the LHC and at RHIC. The analysis of the ALICE low-field data sample from pp collisions at $\sqrt{s} = 13$ TeV [5] shows a hint for an excess of dielectron production in the invariant-mass range $0.15 < m_{\mathrm{ee}} < 0.6$ GeV/$c^2$, with a combined significance of $1.6\,\sigma$, mainly limited by the knowledge of the hadronic decay cocktail at low $p_{\mathrm{T}}$. The excess is most pronounced in the low pair transverse momentum $p_{\mathrm{T,ee}} < 0.4$ GeV/$c$ region, which was made accessible by the lower magnetic field, and, at present, cannot be explained by hadronic bremsstrahlung. Also a calculation of the thermal dielectron yield from a hadronic many-body model that described successfully low-mass dielectron and dimuon production in heavy-ion collisions at the SPS, RHIC and the LHC fails to describe the measured excess. The measurement of the multiplicity dependence of the excess, which may yield important information on the underlying production mechanism, suffers from large statistical and systematic uncertainties and exhibits no clear trend.

The increased data taking capabilities of the upgraded ALICE detector in pp collisions in Run 3 offer a unique opportunity for a major advancement in this direction. The collection of 3 pb$^{-1}$ of minimum bias pp collisions at $\sqrt{s} = 13$ TeV with reduced magnetic field in the ALICE central barrel implies an increase in the number of dielectrons by about a factor 300 over the low-field data from Run 2. This would enable a multi-differential analysis of the dielectron yield as a function of invariant pair mass, pair transverse momentum, and event multiplicity. At the same time, more precise low-$p_{\mathrm{T}}$ measurements of $\pi^0$ and $\eta$ production will result in a reduction of the systematic uncertainty on the hadronic cocktail. The multiplicity-dependent production yield of $\pi^0$ and $\eta$ at low $p_{\mathrm{T}}$ can be measured in the two-photon decay channel, using the well-established photon-conversion method. This will improve the overall systematic uncertainties by about a factor two. Finally, it is also worth noting that this large sample at low magnetic field will be useful to extend to low pair transverse momentum and invariant mass the hadronic and heavy-flavour components of the pp reference for the study of dielectrons in Pb–Pb collisions.

### 2.5 Complementarity with other experiments

This section gives an assessment of the uniqueness and competitiveness of the proposed measurements at the LHC. A summary is reported in Table 1.

**High-multiplicity studies.** The measurements that involve identified light-flavour hadrons, such as pions, kaons, protons, will be accessible only to ALICE in Run 3. This is the case for the strangeness production studies, where the hyperon yields have to be normalised to the pion yields (a normalization to charged particles is prevented by the modified productions of kaons and protons). Also the flow measurements for identified hadrons to precisely test the hydrodynamical expectation of a mass ordering will be accessible only to ALICE in Run 3, although the ATLAS and CMS experiments could carry out partial measurements using neutral kaons and hyperons. The CMS experiment will have pion, kaon and proton identification capability only in Run 4 with the installation of the proposed timing layer in the silicon tracker [76, 77]. However, particle identification will be limited to $p > 0.8$ GeV$/c$: even at large pseudorapidity $|\eta| \approx 1.4$, the minimum accessible transverse momentum will be about 0.4 GeV/$c$. Therefore, the ALICE measurement ($p_{\mathrm{T}} > 0.2$ GeV/$c$) will provide a more complete coverage of the range relevant for the study of the mass ordering of flow observables. The LHCb experiment is in general limited for flow measurements because of the limited pseudorapidity coverage. ALICE can use the central barrel and both backward and forward detectors to limit non-flow effects, which are difficult to eliminate in pp collisions, for example with the three-subevent technique. The search for energy loss effects in high-multiplicity pp (and p–Pb) collisions can be carried out in complementary kinematic regions by ALICE and ATLAS/CMS. The ALICE approach with hadron–jet recoil measurements has unique low $p_{\mathrm{T}}$ access, using reconstructed jets with $p_{\mathrm{T}}$ as low as 5 GeV$/c$ [2]. ATLAS and CMS will mainly use $\gamma$–jet or Z–jet events to search for a modification of the jet/boson momentum fraction for jets with $p_{\mathrm{T}} > 30$ GeV/$c$ and $\gamma$/Z with $p_{\mathrm{T}} > 60$ GeV/$c$ [3].

**Light nuclei, hyper-nuclei, baryon–baryon interactions.** These measurements require the identification of protons and light nuclei (d, $^3$He, $^4$He); therefore, they will be accessible only to ALICE in Run 3. The CMS experiment will have light nuclei identification capability in Run 4 with the installation of the proposed timing layer in the silicon tracker [76, 77]. However, the precise measurements discussed in this document would require extended data-taking with a minimum bias trigger. For example, with the maximum expected minimum-bias rate of 250 kHz, the CMS experiment would have to devote several months per year of data-taking to integrate a luminosity of the order of 100 pb$^{-1}$.

**B mesons, charmonia, jets.** B meson and charmonium measurements down to zero transverse momentum can be carried out only by ALICE and LHCb. The LHCb measurements cover forward rapidity only, while the ALICE measurements will cover both central rapidity (with full B meson reconstruction, J/$\psi$, $\psi$(2S), $\chi_c$) and forward rapidity (non-prompt J/$\psi$, prompt J/$\psi$ and $\psi$(2S)). The CMS and ATLAS experiment measure B-meson production for $p_T > 5$ GeV/$c$ and $> 8$ GeV/$c$, respectively, due to the momentum threshold for muon detection and triggering [78, 79]. A measurement by ALICE at lower $p_T$ would provide the necessary reference for Pb–Pb studies and would enable a study of the dead-cone effect in a kinematic region in which it should be maximal. The production of the X(3872) state is measured for $p_T > 10$ GeV/$c$, while there are good prospects to extend it to lower $p_T$ with ALICE.

**Central exclusive production.** The selection of diffractive events requires a broad pseudorapidity acceptance and low pile-up conditions in order to tag events with only 2–4 tracks at central rapidity and no activity in the backward and forward regions. In addition, the study of the low invariant mass spectrum to search for gluonic components among, for example, the $f_0$ states requires the identification of pions and kaons. Only ALICE and LHCb can contribute to these studies with a complementary rapidity coverage.

**Low-mass dielectrons.** The measurement that we plan to carry out requires access to electrons with transverse momentum down to 75 MeV/$c$ and is only possible with ALICE.

**Table 1:** Summary of the ALICE unique features and of the expected capabilities of the other LHC experiments for the measurements proposed in this document.

| Measurement | ALICE uniqueness | Other experiments |
|---|---|---|
| $\Omega/\pi$ ratio vs. multiplicity | $\pi$, K, p PID $p_{\mathrm{T}} > 0.15$ GeV/$c$ mid-$y$ | — * |
| Flow of $\pi$, K, p at high multiplicity | $\pi$, K, p PID $p_{\mathrm{T}} > 0.15$ GeV/$c$ mid-$y$<br>$p_{\mathrm{T}} < 0.5$ GeV/$c$ crucial for mass ordering | CMS in Run 4 (with proposed timing layer)<br>limited to $p_{\mathrm{T}} > 0.4$ GeV/$c$ at $\lvert\eta\rvert \approx 1.4$ |
| h–jet recoil at high multiplicity | Charged jets $p_{\mathrm{T}}^{\mathrm{jet}} > 15$ GeV/$c$<br>maximum sensitivity to jet $\Delta E$ at low $p_{\mathrm{T}}^{\mathrm{jet}}$ | ATLAS and CMS ($\gamma$/Z–jet with $p_{\mathrm{T}}^{\mathrm{jet}} > 30$ GeV/$c$) |
| Nuclei and hypernuclei | $Z = 2$ nuclei PID $p_{\mathrm{T}} > 0.8$ GeV/$c$ | — * |
| p–hyperon(Y) and Y–Y interaction | $\pi$, K, p PID $p_{\mathrm{T}} > 0.15$ GeV/$c$ mid-$y$ | — |
| B mesons | PID, B mesons $p_{\mathrm{T}} > 0$ mid-$y$<br>Reference for $p_{\mathrm{T}} < 5$ GeV/$c$ B $R_{\mathrm{AA}}$ | ATLAS and CMS ($p_{\mathrm{T}} > 5$ GeV/$c$),<br>LHCb (forward rapidity) |
| Jets and HF jets | Charged jets $p_{\mathrm{T}}^{\mathrm{jet}} > 10$ GeV/$c$<br>Larger dead cone aperture at low radiator $E$ | ATLAS and CMS ($p_{\mathrm{T}} > 30$ GeV/$c$) |
| Charmonia | J/$\psi$, $\psi$(2S) $p_{\mathrm{T}} > 0$ mid- and fwd-$y$,<br>central-forward correlations | ATLAS and CMS ($p_{\mathrm{T}} > 3$ GeV/$c$),<br>LHCb (forward rapidity) |
| Low-mass central diffraction | $\pi$, K, p PID $p_{\mathrm{T}} > 0.15$ GeV/$c$ mid-$y$ | LHCb (forward rapidity) |
| Low-mass dielectrons | e ID $p_{\mathrm{T}} > 75$ MeV/$c$ | — |

* possible in CMS only in Run 4 and with extended running (several months per year) at low rate (min-bias readout rate CMS Run 4: $< 250$ kHz i.e. 2–4 times lower than ALICE).

## 3 Data taking and event selection strategy

After the LS2 upgrade most of the ALICE detectors will support continuous readout and will inspect the full delivered luminosity without a hardware trigger. The exceptions are EMCal, PHOS, TRD, and HMPID. For these detectors, the maximum readout rate in pp collisions ranges from $\sim$10 kHz to $\sim$80 kHz. The baseline plan is to read out HMPID and TRD with a minimum bias or high multiplicity hardware trigger (from the FIT detector), thus inspecting a fraction of the delivered luminosity. The events with TRD data will also be used for the calibration of the space-charge distortions of the TPC drift field using combined ITS-TPC-TRD tracking. EMCal and PHOS have trigger capabilities, and can run in self-triggered mode in order to inspect more than 90% of the delivered luminosity.

For the pp programme, the data taking foresees an approach similar to what will be done during for Pb–Pb [80, 81]: data from all interactions will be shipped to the Online–Offline system ($O^2$) and fully calibrated and reconstructed in two stages, as described in more detail in the next Section. For the low-field data taking (about three weeks), the plan is to reconstruct and use for analysis all of the recorded data. For the full-field part of the pp programme, it will not be possible. As soon as the data are reconstructed, data selection algorithms will skim the events of interest and delete the remaining.

Four main classes of variables can be used separately or in combination to select the events:

1. Event multiplicity and topology: with the use of the ITS tracklets or full tracks it is possible to select events with very high multiplicity (up to 16 times the average multiplicity of pp collisions with $L_{\rm int} = 200$ pb$^{-1}$). This kind of selection relies on the reconstruction of the primary vertex using the first three layers of the ITS. CEP events can be selected using the reconstructed tracks, in combination with a veto on signals in the forward and backward FIT detectors.

2. Particle Identification: after the second stage of the reconstruction, the full calibration of the TPC d$E$/d$x$ information will be available as well as the full information of the tracks timing from TOF. These quantities will be used to select $^3$He and $^4$He nuclei and charmonia in the $e^+e^-$ decay channel. Particle identification from slower detectors like TRD and HMPID will be limited to the events where their information is avalaible. Thanks to the Muon Spectrometer upgrade, muon identification in the forward region will be available for the full recorded luminosity and will be used to select events with forward quarkonium candidates.

3. Decay topology reconstruction: the precise reconstruction of decay vertices of D and B mesons and of $\Omega$ particles using the combined information of TPC and ITS tracking will be used to select events that contain a candidate.

4. Photon and jet reconstruction: the electromagnetic calorimeters EMCal and PHOS will self-trigger on photons and jets. A moderate hardware trigger threshold could be combined with a further software based selection.

A list of the main event selection streams for the full-field pp program is presented in Table 2, where tentative selection criteria and corresponding rejection factors are shown for each stream. The list is not exhaustive but contains the main expected contributions to the total event selection rate. With the rejection factors listed in the table, the total rejection will be about $1.7 \times 10^3$, meaning that 0.06% of the events will be selected, i.e. if the interaction rate is 500 kHz the rate of selected events is 300 Hz. On top of the selected events, a dedicated stream for non-rare events will also be needed as a control sample, for normalisation, for minimum bias physics, and for the TPC space-charge distortion calibration (when TRD data are available). Development is ongoing to optimise the selectivity for such a stream by means e.g. of selection techniques based on time intervals instead of single events. In order to account for these needs and for the possible addition of extra selection streams, a total rejection of about $10^3$ is assumed for the computing resource estimates presented in Section 4.

**Table 2:** Provisional event selection menu and rejection factors for pp data taking in Run 3.

| Stream | Selection | Rejection factor |
|---|---|---|
| High multiplicity | Track(let) multiplicity selection, $N_{ch}/\langle N_{ch}\rangle \geq 7$ | $10^4$ |
| Diffractive | Event topology + $m_{\pi\pi}$ >1 GeV/$c^2$ | $2\times10^4$ |
| Nuclei ($Z$=2) | Loose PID cuts, $n_\sigma(^3\mathrm{He})> -5$ | $10^5$ |
| $\Omega$ or $\overline{\Omega}$ | All cascade topology candidates | $10^4$ |
| Jet and $\gamma$ | EMCal patch energy >20 GeV | $7\times10^3$ |
| Open charm and beauty | Heavy flavour vertexing using PID | $10^4$ |
| Quarkonium (fwd-$y$) | $m_{\mu\mu} > 2$ GeV/$c^2$ | $8\times10^4$ |
| J/$\psi$ (mid-$y$) | 2 e candidates, -3< $n_\sigma$(e)< 4, $n_\sigma$(p)> 2, $n_\sigma(\pi)> 2$ | $2\times10^4$ |

## 4 Data processing and computing requirements

The computing model for Run 3 was presented in the TDR for the Upgrade of the Online-Offline ($O^2$) Computing System [80] and updated in the "Evolution of the $O^2$ system" [81]. Data will be recorded in continuous readout mode and the data stream will be split into time frames with a duration of 10 ms. The reconstructed-data types in Run 3 are the Compressed Time Frame (CTF), which will contain the processed data of all active detectors, and the Analysis Object Data (AOD), which will contain the final track parameters at a given vertex and for a given collision, as well as calorimeter clusters and the signal amplitudes of particle-counting detectors. The detector data will first be processed on the $O^2$ computing facility, including cluster finding and fast-tracking relying on approximate detector calibrations. This processing step, the "synchronous reconstruction", occurs during data taking. The resulting CTFs contain, in a 10 ms time frame, the information from up to 500 (5000) overlapping events of Pb–Pb (pp) collisions at 50 kHz (500 kHz) interaction rate and they will be temporarily stored on a 60 PB disk buffer connected to the $O^2$ facility with fast network. The subsequent CTF processing is done in two "asynchronous reconstruction" passes, analogue to Run 2 RAW-data reconstruction, that produce the analysis-ready AODs. The first pass starts as soon the offline calibrations and alignment are completed and takes place at the Tier0, at the Tier1 centres, and in the unused part of the $O^2$ facility.

The $O^2$ computing facility, composed of First Level Processors (FLPs) and Event Processing Nodes (EPNs), is dimensioned to perform the synchronous processing of the data recorded in Pb–Pb collisions at a 50 kHz peak interaction rate. During pp data taking at an interaction rate of 500 kHz, the synchronous processing requires 12.5% of the EPN resources. The final configuration of the EPN nodes of the $O^2$ facility has recently been defined. The farm will consist of 250 nodes with 2 32-core CPUs and 8 GPUs for each node, totaling about 320 kHS06 of CPU capacity and 2000 GPUs.

Considering that the full capacity of the $O^2$ computing facility (CPU+GPU) is used during the one month of Pb–Pb data taking and during one month after data taking for calibrations, the $O^2$ computing facility is available for other tasks during ten months. Over this period one third of the Pb–Pb asynchronous reconstruction will be performed in the $O^2$ computing facility. Efforts are ongoing to use more GPU resources for asynchronous reconstruction which will allow for a reduction of the impact of Pb–Pb reconstruction and for accommodating the pp synchronous and asynchronous processing on the $O^2$ computing facility.

About 210 days of data taking (7 months) per year at an interaction rate of 500 kHz with 35% LHC efficiency yield an integrated luminosity of 40 pb$^{-1}$ per year. This corresponds to $3.2 \times 10^{12}$ inelastic collisions and 79 PB of total CTF output size (the average CTF size per collision is 25 kB), i.e. $\approx 2.6$ PB per week. During the pp data taking, the synchronous reconstruction will run to assemble the full time frame, carry out TPC track finding using an approximate calibration and partial reconstruction of ITS and TRD to a level that allows precise calibration to be done in subsequent processing steps. Data will be compressed into a CTF format and stored to the $O^2$ disk buffer. The first pp asynchronous pass will begin with a delay of about two weeks after the start of data taking, but four weeks are considered hereafter as a contingency measure. This time is needed to produce and adjust the detector calibration objects so that

the asynchronous processing stage will process the final reconstruction using the final calibration. At this stage, all detectors are included in the reconstruction and global track fitting, primary and secondary vertexing and particle identification are performed. Therefore, at this processing stage it is possible to skim the interesting physics events (see Section 3). At the end of event selection the original CTFs will be further compressed by removing all the information not associated to interesting events.

**Estimate of storage requirements.** The event selection for the full-field data taking, as described in the previous Section, will tag about 0.1% of the events. For each tagged event — and in order to include TPC clusters potentially belonging to the secondary tracks that are not pointing to the primary vertex, e.g. from $\Omega$ or hyper-nuclei decays — all clusters attached to tracks that point to the tagged primary vertex within a fiducial region of $\pm$30 cm along the beam direction are kept. Therefore, with an interaction rate of 500 kHz, 12 events per selected event will be kept, which corresponds to 1.2% of the original CTF size. For the total of $L_{\rm int} = 200$ pb$^{-1}$, the selected CTF size amounts to about 5 PB. For the low-field minimum bias data sample, the total data volume, corresponding to $L_{\rm int} = 3$ pb$^{-1}$, amounts to about 8 PB (30% larger event size with respect to the full-field case is considered, due to the lower $p_{\rm T}$ cutoff). The total amount of tape storage needed for the full pp data sample outlined in this document amounts to 13 PB. Assuming the AOD size to be about 10% of the CTF size, the disk volume needed to store the AODs amounts to about 3 PB for two reconstruction passes.

**Estimate of O$^2$ computing requirements.** The processing resources needed for the asynchronous pass can be estimated from the Table 4.3 of Ref. [81], where a total of 8285 s are considered for the processing of 1000 Pb–Pb collisions on a single worker node with a CPU capacity of 22.7 HS06. By scaling from Pb–Pb to pp particle multiplicity, and taking into account a contingency factor of 10% for the larger overhead expected in the pp event reconstruction, the computing power for the pp asynchronous reconstruction pass could be assessed at about 2.65 HS06$\times$s per collision. Figure 8 (upper panel) shows the maximum accumulated CTF size (blue line) as a function of the processing capacity effectively available for the pp asynchronous pass, in the hypothesis that the asynchronous pass starts four weeks after the start of pp data taking. Here, a pp data taking period of 210 days with an overall LHC efficiency of 35% at an interaction rate of 500 kHz is considered. During years following a Pb–Pb run, according to the Run 3 computing model, 2/3 of the Pb–Pb CTF files will be kept on the O$^2$ disk buffer and processed for most of the year, while 1/3 will be moved to Tier1s in the months following the data taking and will be processed there, making available 20 PB of disk buffer. The maximum accumulated CTF size is below the currently foreseen available disk buffer size of 20 PB if the processing capacity is at least 450 kHS06. The lower panel of Fig. 8 shows the profile in time, during a yearly pp run at 500 kHz interaction rate, of the total CTF data size (grey line) produced by the synchronous processing of all collisions and of the total occupied disk buffer (blue line) when a 450 kHS06 processing capacity is employed for the first asynchronous processing and event selection at the O$^2$ computing facility. More accurate estimates of the needed computing resources will be available in the coming months, after the Production Readiness Review of the reconstruction software. While the asynchronous reconstruction software for the CPUs is almost finalized, the version to exploit the GPU features is under development. A factor of about two reduction of the CPU capacity requirement of 450 kHS06s for the pp asynchronous pass may be confidently expected by offloading part of the processing to GPUs and by optimizing the present software. Under this assumption, the processing capacity of the O$^2$ computing facility will allow to accommodate the pp data acquisition at 500 kHz (estimated as 12.5% of the total O$^2$ facility processing capacity) and their offline reduction in the first year of Run 3. In the following years, from 2023, the pp asynchronous pass would be accommodated by processing on the Tier-0 a fraction of the Pb–Pb sample larger than the originally-planned 1/3. This would require a moderate additional increase of about 5% per year from 2023 of the ALICE CPU resources at the Tier-0 with respect the projected growth of 15% per year. Within this budget and with further software optimization, an increase of the readout rate to 1 MHz will be feasible starting from 2024.

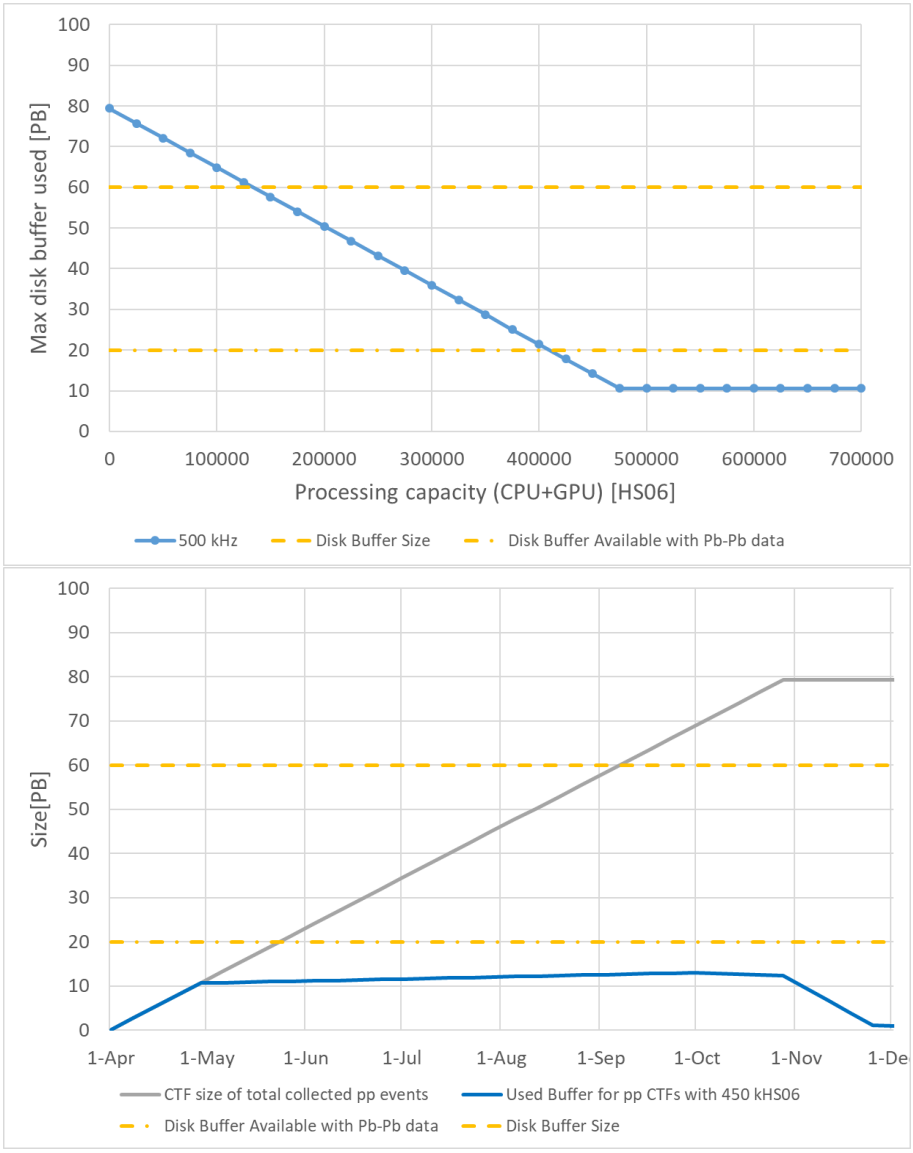


**Fig. 8:** Upper panel: Required disk buffer as a function of the processing capacity employed for the asynchronous reconstruction of the pp data collected at 500 kHz interaction rate, under the assumption that the processing will start four weeks after the beginning of data taking. Lower panel: Total CTF data size (grey line) produced by the synchronous processing of the 500 kHz pp interaction rate collisions as a function of time in the year and total occupied disk buffer (blue line) when 450 kHS06 processing capacity is used for the asynchronous reconstruction of the data. In both panels: The dot-dashed (dashed) horizontal line indicates the $O^2$ disk buffer available in years preceded (not preceded) by a Pb–Pb run.

**Estimates of GRID computing requirements.** The reduced pp CTFs will be exported and subsequently processed for the second asynchronous pass on the Tier0 and the Tier1s, while the simulation could be run on all Tier levels. The CPU resources necessary to perform the second asynchronous pass of the full-field pp data will be marginal (13 kHS06 for 90 days per year), because the events are highly selected, whereas the two asynchronous passes for the low-field data sample (for which no event selection is foreseen) require 55 kHS06 for 175 days per pass, which corresponds to about 10% of the CPU capacity needed for the asynchronous pass of the Pb–Pb data sample.

A first estimate of the CPU and disk resources for Monte Carlo (MC) simulations, considering a number of simulated events equal to that of selected data events and the usage of MC-embedding for the pileup,

amounts to about 90 kHS06 and a few hundred TB for each full-field data taking year. Sharing the needed 90 kHS06 among the 3 Tier levels, the total CPU requirement will amount to about 6% of the Tiers CPU capacity. The estimate of the computing resource needs for the simulation anchored to the low-field data sample depends on the ratio between generated and collected events. If this ratio is kept at the level of 1%, the required CPU capacity will correspond to about 10% of the CPU capacity needed for the simulation of Pb–Pb data sample per year. In summary, the overall impact of the high-energy pp programme on the GRID computing will be of about an additional 10% per year from 2023 with respect to the projected resources.

## 5 Radiation load estimates

The extended pp programme proposed in this document will largely increase the total radiation dose on the various components of the ALICE apparatus during Run 3, because the total number of charged particles per unit of rapidity for pp collisions at $\sqrt{s} = 14$ TeV with $L_{\rm int} = 200$ pb$^{-1}$ is about 3 times larger than for Pb–Pb collisions at $\sqrt{s_{\rm NN}} = 5.5$ TeV with $L_{\rm int} = 6.5$ nb$^{-1}$ (half of the goal for Runs 3+4).

The radiation dose was estimated using detailed simulations of the ALICE apparatus, including all passive materials, based on the FLUKA transport package [82] and are reported in Ref. [83]. Table 3 reports the results for Runs 3+4 with the original running scenario and with an extended scenario that includes pp collisions at $\sqrt{s} = 14$ TeV with $L_{\rm int} = 200$ pb$^{-1}$ and p–Pb data taking extended to the target of 0.5 pb$^{-1}$ proposed by the HL-LHC workshop WG5 [3][14]. The radiation from beam-induced background during the LHC pp operation is also included: this background contributes to the Total Integrated Dose (TID) only if ALICE takes data (detectors powered), while it contributes to the Non-Ionizing Energy Loss (NIEL) also if the detectors are off. The background rate scales with the vacuum pressure in the long straight section of the LHC (LSS2) nearby the ALICE interaction point. In the tables, the values outside brackets are obtained with background level corresponding to the average vacuum pressure measured during Run 2 ($10^{-10}$ mbar): in this case the contribution from the background is negligible with respect to that from the collisions. However, since the dynamic vacuum pressure is very sensitive to the beam conditions, which will change significantly after LS2, a more conservative value of $2.3 \times 10^{-9}$ mbar is also considered and leads to the values reported in brackets. The values for the TID and NIEL increase by a factor about 4 with the extended programme. The high-energy hadron fluence and charged-particle fluence rates reported in the tables for Pb–Pb collisions at $\sqrt{s_{\rm NN}} = 5.5$ TeV at the interaction rate of 50 kHz are larger by a factor about 2 with respect to those for pp collisions at $\sqrt{s} = 14$ TeV at the interaction rate of 500 kHz (not reported in the tables). For completeness, also the radiation values for one of the years of Run 3 with extended pp running and a Pb–Pb run are reported, see Table 4.

The resulting values for TID and NIEL for Runs 3+4 in the detectors that are closest to the interaction point (ITS L0, L1, L2, and MFT) are similar to those for which the ALPIDE sensor of the ITS and MFT was validated with irradiation tests for the Production Readiness Review [84]. More precisely, the ALPIDE was validated for a radiation load of up to $1.7 \times 10^{13}$ 1 MeV Neq (NIEL) and about 400 krad. The results indicated that, after receiving such a radiation dose, the ALPIDE chip preserves its full functionality and detection performance, but the operational margin is reduced by about one third. Concerning the radiation damage induced by TID, it is important to note that the vast majority of the measurements on ALPIDE samples was carried out with dose rates (krad/s) that are 1000 times larger than those from LHC collisions. Since radiation damage from TID is dose-rate sensitive, a few measurements were carried out at lower dose rate, but still 20 times higher than from collisions. The results of these measurements indicated that the ALPIDE chip preserves its performance even when irradiated at doses in excess of 2 Mrad. However, the results at 2 Mrad are relative to measurements done with only a handful of circuits. As for the Readout Units (RU), their radiation tolerance is of 10 krad, which is one

[14] The discussion of this extended p–Pb programme goes beyond the scope of the present document and will be part of a future proposal for the specific scheduling of the LHC heavy-ion periods of Runs 3 and 4.

**Table 3:** TID and NIEL weighted 1-MeV-neq fluence for the original running scenario of Run 3 and Run 4 (13 $nb^{-1}$ Pb–Pb + 50 $nb^{-1}$ p–Pb + 6 $pb^{-1}$ pp collisions) and for the extended scenario (13 $nb^{-1}$ Pb–Pb + 500 $nb^{-1}$ p–Pb + 200 $pb^{-1}$ pp collisions). The high-energy hadron fluence rate and charged-particle fluence rate for Pb–Pb collisions at an interaction rate of 50 kHz are also reported. The numbers correspond to the average values in the given $z$ interval while the numbers in brackets refer to the peak value inside this interval. The values are obtained with the upgraded ITS and beam pipe geometry and they are reported only for the ITS layer (L0) and MFT disk (D2) with the highest dose, as well as for the readout units (RU) and the FIT1 detector. From Ref. [83].

| Element | $r$ (cm) | $z$ (cm) | TID (krad) | TID (krad) ext. | 1-MeV-neq ($cm^{-2}$) | 1-MeV-neq ($cm^{-2}$) ext. | Charged part. ($kHz/cm^2$) | >20 MeV had. ($kHz/cm^2$) |
|---|---|---|---|---|---|---|---|---|
| ITS L0 | 2.2 | −13.5, 13.5 | 50.9 | 179.7 | $1.0 \times 10^{12}$ | $3.6 \times 10^{12}$ | 709 | 708 |
| | | | [73.1] | [217.0] | [$1.2 \times 10^{12}$] | [$3.8 \times 10^{12}$] | [715] | [712] |
| ITS RU | 100 | 330 | 0.18 | 0.63 | $9.8 \times 10^{9}$ | $3.5 \times 10^{10}$ | 2.0 | 0.93 |
| | | | [0.21] | [0.68] | [$1.2 \times 10^{10}$] | [$3.7 \times 10^{10}$] | [2.1] | [0.95] |
| MFT D2 | 3.0 | −66 | 41.4 | 147.7 | $6.2 \times 10^{11}$ | $2.3 \times 10^{12}$ | 433 | 380 |
| | | | [51.0] | [163.7] | [$8.0 \times 10^{11}$] | [$3.0 \times 10^{12}$] | [526] | [383] |
| MFT RU | 132 | -438 | 0.041 | 0.14 | $5.3 \times 10^{9}$ | $1.9 \times 10^{10}$ | 0.42 | 0.4 |
| | | | [0.052] | [0.16] | [$7.0 \times 10^{9}$] | [$2.0 \times 10^{10}$] | [0.47] | [0.42] |
| FIT1 | 5 | −80 | 15.9 | 55.7 | $3.4 \times 10^{11}$ | $1.2 \times 10^{12}$ | 169 | 143 |
| | | | [27.7] | [75.5] | [$4.7 \times 10^{11}$] | [$1.3 \times 10^{12}$] | [233] | [144] |

**Table 4:** TID and NIEL weighted 1-MeV-neq fluence for one year in Run 3 with 3 $nb^{-1}$ Pb–Pb + 45 $pb^{-1}$ pp collisions. Adapted from Ref. [83].

| Element | $r$ (cm) | $z$ (cm) | TID (krad) | 1-MeV-neq ($cm^{-2}$) |
|---|---|---|---|---|
| ITS L0 | 2.2 | −13.5, 13.5 | 32.8 | $6.6 \times 10^{11}$ |
| | | | [40.8] | [$7.2 \times 10^{11}$] |
| ITS RU | 100 | 330 | 0.12 | $6.3 \times 10^{9}$ |
| | | | [0.13] | [$6.8 \times 10^{9}$] |
| MFT D2 | 3.0 | −66 | 26.8 | $4.0 \times 10^{11}$ |
| | | | [30.3] | [$4.5 \times 10^{11}$] |
| MFT RU | 132 | -438 | 0.026 | $3.4 \times 10^{9}$ |
| | | | [0.03] | [$3.9 \times 10^{9}$] |
| FIT1 | 5 | −80 | 10.2 | $2.2 \times 10^{11}$ |
| | | | [14.5] | [$2.6 \times 10^{11}$] |

order of magnitude larger than the expected load reported in Table 3.

In conclusion, the ALPIDE chip was validated to radiation values well above (factor $\sim 5$ for hadron fluency and $\sim 2$ for TID) those projected for Run 3 and Run 4, including the extended pp campaign. Measurements carried out on a small set of circuits at more realistic dose rates indicate that the safety margin might be significantly larger.

## Acknowledgements

The ALICE Collaboration would like to thank all its engineers and technicians for their invaluable contributions to the construction of the experiment and the CERN accelerator teams for the outstanding performance of the LHC complex. The ALICE Collaboration gratefully acknowledges the resources and support provided by all Grid centres and the Worldwide LHC Computing Grid (WLCG) collaboration.

The ALICE Collaboration acknowledges the following funding agencies for their support in building and running the ALICE detector: A. I. Alikhanyan National Science Laboratory (Yerevan Physics Institute) Foundation (ANSL), State Committee of Science and World Federation of Scientists (WFS), Armenia; Austrian Academy of Sciences, Austrian Science Fund (FWF): [M 2467-N36] and Nationalstiftung für Forschung, Technologie und Entwicklung, Austria; Ministry of Communications and High Technologies, National Nuclear Research Center, Azerbaijan; Conselho Nacional de Desenvolvimento Científico e Tecnológico (CNPq), Financiadora de Estudos e Projetos (Finep), Fundação de Amparo à Pesquisa do Estado de São Paulo (FAPESP) and Universidade Federal do Rio Grande do Sul (UFRGS), Brazil; Ministry of Education of China (MOEC) , Ministry of Science & Technology of China (MSTC) and National Natural Science Foundation of China (NSFC), China; Ministry of Science and Education and Croatian Science Foundation, Croatia; Centro de Aplicaciones Tecnológicas y Desarrollo Nuclear (CEADEN), Cubaenergía, Cuba; Ministry of Education, Youth and Sports of the Czech Republic, Czech Republic; The Danish Council for Independent Research | Natural Sciences, the VILLUM FONDEN and Danish National Research Foundation (DNRF), Denmark; Helsinki Institute of Physics (HIP), Finland; Commissariat à l'Energie Atomique (CEA) and Institut National de Physique Nucléaire et de Physique des Particules (IN2P3) and Centre National de la Recherche Scientifique (CNRS), France; Bundesministerium für Bildung und Forschung (BMBF) and GSI Helmholtzzentrum für Schwerionenforschung GmbH, Germany; General Secretariat for Research and Technology, Ministry of Education, Research and Religions, Greece; National Research, Development and Innovation Office, Hungary; Department of Atomic Energy Government of India (DAE), Department of Science and Technology, Government of India (DST), University Grants Commission, Government of India (UGC) and Council of Scientific and Industrial Research (CSIR), India; Indonesian Institute of Science, Indonesia; Centro Fermi - Museo Storico della Fisica e Centro Studi e Ricerche Enrico Fermi and Istituto Nazionale di Fisica Nucleare (INFN), Italy; Institute for Innovative Science and Technology , Nagasaki Institute of Applied Science (IIST), Japanese Ministry of Education, Culture, Sports, Science and Technology (MEXT) and Japan Society for the Promotion of Science (JSPS) KAKENHI, Japan; Consejo Nacional de Ciencia (CONACYT) y Tecnología, through Fondo de Cooperación Internacional en Ciencia y Tecnología (FONCICYT) and Dirección General de Asuntos del Personal Academico (DGAPA), Mexico; Nederlandse Organisatie voor Wetenschappelijk Onderzoek (NWO), Netherlands; The Research Council of Norway, Norway; Commission on Science and Technology for Sustainable Development in the South (COMSATS), Pakistan; Pontificia Universidad Católica del Perú, Peru; Ministry of Science and Higher Education, National Science Centre and WUT ID-UB, Poland; Korea Institute of Science and Technology Information and National Research Foundation of Korea (NRF), Republic of Korea; Ministry of Education and Scientific Research, Institute of Atomic Physics and Ministry of Research and Innovation and Institute of Atomic Physics, Romania; Joint Institute for Nuclear Research (JINR), Ministry of Education and Science of the Russian Federation, National Research Centre Kurchatov Institute, Russian Science Foundation and Russian Foundation for Basic Research, Russia; Ministry of Education, Science, Research and Sport of the Slovak Republic, Slovakia; National Research Foundation of South Africa, South Africa; Swedish Research Council (VR) and Knut & Alice Wallenberg Foundation (KAW), Sweden; European Organization for Nuclear Research, Switzerland; Suranaree University of Technology (SUT), National Science and Technology Development Agency (NSDTA) and Office of the Higher Education Commission under NRU project of Thailand, Thailand; Turkish Atomic Energy Agency (TAEK), Turkey; National Academy of Sciences of Ukraine, Ukraine; Science and Technology Facilities Council (STFC), United Kingdom; National Science Foundation of the United States of America (NSF) and United States Department of Energy, Office of Nuclear Physics (DOE NP), United States of America.

## References

[1] **ALICE** Collaboration, B. Abelev *et al.*, "Upgrade of the ALICE Experiment: Letter Of Intent", *J. Phys. G* **41** (2014) 087001.

[2] **ALICE** Collaboration, "ALICE upgrade physics performance studies for 2018 Report on HL/HE-LHC physics", ALICE-PUBLIC-2019-001. https://cds.cern.ch/record/2661798.

[3] Z. Citron *et al.*, "Future physics opportunities for high-density QCD at the LHC with heavy-ion and proton beams", in *HL/HE-LHC Workshop: Workshop on the Physics of HL-LHC, and Perspectives at HE-LHC Geneva, Switzerland, June 18-20, 2018*. 2018. arXiv:1812.06772 [hep-ph].

[4] L. Cunqueiro and M. Pł oskoń, "Searching for the dead cone effects with iterative declustering of heavy-flavor jets", *Phys. Rev. D* **99** no. 7, (2019) 074027, arXiv:1812.00102 [hep-ph].

[5] **ALICE** Collaboration, S. Acharya *et al.*, "Soft-dielectron excess in proton-proton collisions at $\sqrt{s}$ = 13 TeV", arXiv:2005.14522 [nucl-ex].

[6] **ALICE** Collaboration, B. Abelev *et al.*, "Long-range angular correlations on the near and away side in p–Pb collisions at $\sqrt{s_{\rm NN}} = 5.02$ TeV", *Phys. Lett.* **B719** (2013) 29–41, arXiv:1212.2001 [nucl-ex].

[7] **ATLAS** Collaboration, G. Aad *et al.*, "Observation of associated near-side and away-side long-range correlations in $\sqrt{s_{\rm NN}} = 5.02$ TeV p–Pb collisions with the ATLAS detector", *Phys. Rev. Lett.* **110** no. 18, (2013) 182302, arXiv:1212.5198 [hep-ex].

[8] **CMS** Collaboration, V. Khachatryan *et al.*, "Observation of Long-Range Near-Side Angular Correlations in Proton-Proton Collisions at the LHC", *JHEP* **09** (2010) 091, arXiv:1009.4122 [hep-ex].

[9] A. Bzdak, B. Schenke, P. Tribedy, and R. Venugopalan, "Initial state geometry and the role of hydrodynamics in proton-proton, proton-nucleus and deuteron-nucleus collisions", *Phys. Rev.* **C87** no. 6, (2013) 064906, arXiv:1304.3403 [nucl-th].

[10] **ALICE** Collaboration, J. Adam *et al.*, "Two-pion femtoscopy in p-Pb collisions at $\sqrt{s_{\rm NN}} = 5.02$ TeV", *Phys. Rev. C* **91** (2015) 034906, arXiv:1502.00559 [nucl-ex].

[11] **ALICE** Collaboration, B. Abelev *et al.*, "Transverse sphericity of primary charged particles in minimum bias proton-proton collisions at $\sqrt{s} = 0.9$, 2.76 and 7 TeV", *Eur. Phys. J. C* **72** (2012) 2124, arXiv:1205.3963 [hep-ex].

[12] **ALICE** Collaboration, S. Acharya *et al.*, "Charged-particle production as a function of multiplicity and transverse spherocity in pp collisions at $\sqrt{s} = 5.02$ and 13 TeV", *Eur. Phys. J. C* **79** no. 10, (2019) 857, arXiv:1905.07208 [nucl-ex].

[13] S. Deb, S. Tripathy, G. Sarwar, R. Sahoo, and J.-e. Alam, "Deciphering QCD dynamics in small collision systems using event shape and final state multiplicity at the Large Hadron Collider", arXiv:2007.04194 [hep-ph].

[14] A. N. Mishra, G. Paić, C. Pajares, R. Scharenberg, and B. Srivastava, "Sudden increase in the degrees of freedom in dense QCD matter", arXiv:2006.10169 [hep-ph].

[15] **ALICE** Collaboration, J. Adam *et al.*, "Enhanced production of multi-strange hadrons in high-multiplicity proton-proton collisions", *Nature Phys.* **13** (2017) 535–539, arXiv:1606.07424 [nucl-ex].

[16] **ALICE** Collaboration, S. Acharya *et al.*, "Multiplicity dependence of (multi-)strange hadron production in proton-proton collisions at $\sqrt{s}$ = 13 TeV", *Eur. Phys. J. C* **80** no. 2, (2020) 167, arXiv:1908.01861 [nucl-ex].

[17] Y. Kanakubo, Y. Tachibana, and T. Hirano, "Unified description of hadron yield ratios from dynamical core-corona initialization", *Physical Review C* **101** no. 2, (Feb, 2020) . http://dx.doi.org/10.1103/PhysRevC.101.024912.

[18] T. Pierog *et al.*, "Collective hadronization and air showers: can LHC data solve the muon puzzle?", *PoS* **ICRC2019** (2019) 387. https://pos.sissa.it/358/387/.

[19] **ALICE** Collaboration, S. Acharya *et al.*, "Investigations of Anisotropic Flow Using Multiparticle Azimuthal Correlations in pp, p-Pb, Xe-Xe, and Pb-Pb Collisions at the LHC", *Phys. Rev. Lett.* **123** no. 14, (2019) 142301, arXiv:1903.01790 [nucl-ex].

[20] **ALICE** Collaboration, S. Acharya *et al.*, "Investigation of the p-$\Sigma^0$ interaction via femtoscopy in pp collisions", *Phys. Lett. B* **805** (2020) 135419, arXiv:1910.14407 [nucl-ex].

[21] **ALICE** Collaboration, J. Adam *et al.*, "Centrality dependence of particle production in p-Pb collisions at $\sqrt{s_{\rm NN}}$ = 5.02 TeV", *Phys. Rev.* **C91** no. 6, (2015) 064905, arXiv:1412.6828 [nucl-ex].

[22] **ALICE** Collaboration, S. Acharya *et al.*, "Constraints on jet quenching in p-Pb collisions at $\sqrt{s_{NN}}$ = 5.02 TeV measured by the event-activity dependence of semi-inclusive hadron-jet distributions", *Phys. Lett.* **B783** (2018) 95–113, arXiv:1712.05603 [nucl-ex].

[23] **AMS** Collaboration, M. Aguilar *et al.*, "First Result from the Alpha Magnetic Spectrometer on the International Space Station: Precision Measurement of the Positron Fraction in Primary Cosmic Rays of 0.5–350 GeV", *Phys. Rev. Lett.* **110** (2013) 141102.

[24] **GAPS** Collaboration, R. A. Ong *et al.*, "The GAPS Experiment to Search for Dark Matter using Low-energy Antimatter", *PoS* **ICRC2017** (2018) 914, arXiv:1710.00452 [astro-ph.IM].

[25] V. Poulin, P. Salati, I. Cholis, M. Kamionkowski, and J. Silk, "Where do the AMS-02 antihelium events come from?", *Phys. Rev.* **D99** no. 2, (2019) 023016, arXiv:1808.08961 [astro-ph.HE].

[26] **ALICE** Collaboration, S. Acharya *et al.*, "Production of deuterons, tritons, $^3$He nuclei and their antinuclei in pp collisions at $\sqrt{s}$ = 0.9, 2.76 and 7 TeV", *Phys. Rev.* **C97** no. 2, (2018) 024615, arXiv:1709.08522 [nucl-ex].

[27] C. Loizides, J. Kamin, and D. d'Enterria, "Improved Monte Carlo Glauber predictions at present and future nuclear colliders", *Phys. Rev.* **C97** no. 5, (2018) 054910, arXiv:1710.07098 [nucl-ex]. [erratum: Phys. Rev.C99,no.1,019901(2019)].

[28] K.-J. Sun, C. M. Ko, and B. Dönigus, "Suppression of light nuclei production in collisions of small systems at the Large Hadron Collider", *Phys. Lett. B* **792** (2019) 132–137, arXiv:1812.05175 [nucl-th].

[29] V. Vovchenko, B. Dönigus, and H. Stoecker, "Multiplicity dependence of light nuclei production at LHC energies in the canonical statistical model", *Phys. Lett. B* **785** (2018) 171–174, arXiv:1808.05245 [hep-ph].

[30] **ALICE** Collaboration, J. Adam *et al.*, "$^3_\Lambda$H and $^{\overline{3}}_{\overline{\Lambda}}\overline{\rm H}$ production in Pb-Pb collisions at $\sqrt{s_{\rm NN}} = 2.76$ TeV", *Phys. Lett. B* **754** (2016) 360–372, arXiv:1506.08453 [nucl-ex].

[31] F. Bellini, K. Blum, A. P. Kalweit, and M. Puccio, "On coalescence as the origin of nuclei in hadronic collisions", arXiv:2007.01750 [nucl-th].

[32] **ALICE** Collaboration, S. Acharya *et al.*, "p-p, p-Λ and Λ-Λ correlations studied via femtoscopy in pp reactions at $\sqrt{s}$ = 7 TeV", *Phys. Rev. C* **99** no. 2, (2019) 024001, arXiv:1805.12455 [nucl-ex].

[33] **ALICE** Collaboration, S. Acharya *et al.*, "First Observation of an Attractive Interaction between a Proton and a Cascade Baryon", *Phys. Rev. Lett.* **123** no. 11, (2019) 112002, arXiv:1904.12198 [nucl-ex].

[34] **ALICE** Collaboration, S. Acharya *et al.*, "Scattering studies with low-energy kaon-proton femtoscopy in proton-proton collisions at the LHC", *Phys. Rev. Lett.* **124** no. 9, (2020) 092301, arXiv:1905.13470 [nucl-ex].

[35] **ALICE** Collaboration, S. Acharya *et al.*, "Study of the Λ-Λ interaction with femtoscopy correlations in pp and p-Pb collisions at the LHC", *Phys. Lett. B* **797** (2019) 134822, arXiv:1905.07209 [nucl-ex].

[36] **ALICE** Collaboration, S. Acharya *et al.*, "A new laboratory to study hadron-hadron interactions", arXiv:2005.11495 [nucl-ex].

[37] F. Eisele, H. Filthuth, W. Foehlisch, V. Hepp, and G. Zech, "Elastic $\Sigma^+ - p$ scattering at low energies", *Phys. Lett.* **B37** (1971) 204–206.

[38] R. S. Hayano *et al.*, "Observation of a Bound State of $^{4}_{\Sigma}$He Hypernucleus", *Phys. Lett.* **B231** (1989) 355–358.

[39] L. Tang *et al.*, "Observations of hyperon–nucleus systems produced on $^{12}$C and $^{7}$Li targets using the $(K^-, \pi^+)$ reaction at 715 MeV/$c$", *Phys. Rev.* **C38** (1988) 846–853.

[40] C. Batty, E. Friedman, and A. Gal, "Density dependence of the Σ nucleus optical potential derived from $\Sigma^-$ atom data", *Phys. Lett.* **B 335** (1994) 273 – 278.

[41] J. Mareš, E. Friedman, A. Gal, and B. Jenning, "Constraints on Σ-nucleus dynamics from dirac phenomenology of $\Sigma^-$ atoms", *Nucl. Phys.* **A594** no. 3, (1995) 311 – 324.

[42] M. M. Nagels, T. A. Rijken, and Y. Yamamoto, "Extended-soft-core baryon–baryon model ESC16. II. Hyperon–nucleon interactions", *Phys. Rev.* **C99** (2019) 044003.

[43] J. Haidenbauer, S. Petschauer, N. Kaiser, U. G. Meissner, A. Nogga, and W. Weise, "Hyperon–nucleon interaction at next-to-leading order in chiral effective field theory", *Nucl. Phys.* **A915** (2013) 24–58.

[44] S. Gongyo *et al.*, "Most Strange Dibaryon from Lattice QCD", *Phys. Rev. Lett.* **120** no. 21, (2018) 212001, arXiv:1709.00654 [hep-lat].

[45] J. Haidenbauer, "Exploring the Λ-deuteron interaction via correlations in heavy-ion collisions", arXiv:2005.05012 [nucl-th].

[46] **HAL QCD** Collaboration, T. Iritani *et al.*, "$N\Omega$ dibaryon from lattice QCD near the physical point", *Phys. Lett.* **B792** (2019) 284–289, arXiv:1810.03416 [hep-lat].

[47] T. Sekihara, Y. Kamiya, and T. Hyodo, "$N\Omega$ interaction: meson exchanges, inelastic channels, and quasibound state", *Phys. Rev.* **C98** no. 1, (2018) 015205, arXiv:1805.04024 [hep-ph].

[48] D. Logoteta, I. Vidana, and I. Bombaci, "Impact of chiral hyperonic three-body forces on neutron stars", *Eur. Phys. J. A* **55** no. 11, (2019) 207, arXiv:1906.11722 [nucl-th].

[49] S. Mrowczynski and P. Slon, "Hadron-Deuteron Correlations and Production of Light Nuclei in Relativistic Heavy-Ion Collisions", arXiv:1904.08320 [nucl-th].

[50] J. H. Stiller, "Full kinematic reconstruction of charged B mesons with the upgraded Inner Tracking System of the ALICE Experiment", 2016. https://cds.cern.ch/record/2153601. Presented 11 May 2016.

[51] **ALICE** Collaboration, B. Abelev *et al.*, "Technical Design Report for the Upgrade of the ALICE Inner Tracking System", *J. Phys.* **G41** (2014) 087002.

[52] M. Cacciari, S. Frixione, and P. Nason, "The $p_{\mathrm{T}}$ spectrum in heavy flavor photoproduction", *JHEP* **03** (2001) 006, arXiv:hep-ph/0102134 [hep-ph].

[53] M. Cacciari, M. Greco, and P. Nason, "The $p_{\mathrm{T}}$ spectrum in heavy flavor hadroproduction", *JHEP* **05** (1998) 007, arXiv:hep-ph/9803400 [hep-ph].

[54] T. Sjostrand, S. Mrenna, and P. Z. Skands, "PYTHIA 6.4 Physics and Manual", *JHEP* **05** (2006) 026, arXiv:hep-ph/0603175 [hep-ph].

[55] P. Z. Skands, "Tuning Monte Carlo Generators: The Perugia Tunes", *Phys. Rev.* **D82** (2010) 074018, arXiv:1005.3457 [hep-ph].

[56] **LHCb** Collaboration, R. Aaij *et al.*, "Measurement of the ratio of prompt $\chi_c$ to $\mathrm{J}/\psi$ production in pp collisions at $\sqrt{s} = 7$ TeV", *Phys.Lett.B* **718** (2012) 431–440, arXiv:1204.1462 [hep-ex].

[57] **CMS** Collaboration, S. Chatrchyan *et al.*, "Measurement of the X(3872) production cross section via decays to $\mathrm{J}/\psi\pi^+\pi^-$ in pp collisions at $\sqrt{s} = 7$ TeV", *JHEP* **04** (2013) 154, arXiv:1302.3968 [hep-ex].

[58] J. P. Lansberg, "Real next-to-next-to-leading-order QCD corrections to $\mathrm{J}/\psi$ and $\Upsilon$ hadroproduction in association with a photon", *Phys. Lett.* **B679** (2009) 340–346, arXiv:0901.4777 [hep-ph].

[59] **LHCb** Collaboration, R. Aaij *et al.*, "Observation of double charm production involving open charm in pp collisions at $\sqrt{s} = 7$ TeV", *JHEP* **06** (2012) 141, arXiv:1205.0975 [hep-ex]. [Addendum: JHEP03,108(2014)].

[60] C. J. Morningstar and M. J. Peardon, "The Glueball spectrum from an anisotropic lattice study", *Phys. Rev.* **D60** (1999) 034509, arXiv:hep-lat/9901004 [hep-lat].

[61] W. Ochs, "The Status of Glueballs", *J. Phys. G* **40** (2013) 043001, arXiv:1301.5183 [hep-ph].

[62] M. G. Albrow, T. D. Coughlin, and J. R. Forshaw, "Central Exclusive Particle Production at High Energy Hadron Colliders", *Prog.Part.Nucl.Phys.* **65** (2010) 149–184, arXiv:1006.1289 [hep-ph].

[63] **STAR** Collaboration, R. Sikora, "Recent results on Central Exclusive Production with the STAR detector at RHIC", in *Diffraction and Low-x 2018 (Difflowx2018) Reggio Calabria, Italy, August 26-September 1, 2018*. 2018. arXiv:1811.03315 [hep-ex].

[64] **CDF** Collaboration, T. A. Aaltonen *et al.*, "Measurement of central exclusive $\pi^+\pi^-$ production in $p\bar{p}$ collisions at $\sqrt{s} = 0.9$ and 1.96 TeV at CDF", *Phys. Rev.* **D91** no. 9, (2015) 091101, arXiv:1502.01391 [hep-ex].

[65] **CMS** Collaboration, V. Khachatryan *et al.*, "Exclusive and semi-exclusive pi+pi- production in proton-proton collisions at sqrt(s) = 7 TeV", arXiv:1706.08310 [hep-ex].

[66] V. Crede and C. A. Meyer, "The Experimental Status of Glueballs", *Prog. Part. Nucl. Phys.* **63** (2009) 74–116, arXiv:0812.0600 [hep-ex].

[67] T. Bauer, R. Spital, D. Yennie, and F. Pipkin, "The Hadronic Properties of the Photon in High-Energy Interactions", *Rev. Mod. Phys.* **50** (1978) 261. [Erratum: Rev.Mod.Phys. 51, 407 (1979)].

[68] J. R. Forshaw and D. Ross, *Quantum chromodynamics and the pomeron*, vol. 9. Cambridge University Press, 1, 2011.

[69] **STAR** Collaboration, L. Adamczyk *et al.*, "Single Spin Asymmetry $A_N$ in Polarized Proton-Proton Elastic Scattering at $\sqrt{s} = 200$ GeV", *Phys. Lett. B* **719** (2013) 62–69, arXiv:1206.1928 [nucl-ex].

[70] C. Ewerz, P. Lebiedowicz, O. Nachtmann, and A. Szczurek, "Helicity in proton–proton elastic scattering and the spin structure of the pomeron", *Phys. Lett. B* **763** (2016) 382–387, arXiv:1606.08067 [hep-ph].

[71] C. Ewerz, M. Maniatis, and O. Nachtmann, "A Model for Soft High-Energy Scattering: Tensor Pomeron and Vector Odderon", *Annals Phys.* **342** (2014) 31–77, arXiv:1309.3478 [hep-ph].

[72] L. A. Harland-Lang, V. A. Khoze, and M. G. Ryskin, "SuperChic2: a New Monte Carlo for Central Exclusive Production", *Acta Phys. Polon. Supp.* **8** (2015) 751–756.

[73] V. Gonçalves, G. Sampaio dos Santos, and C. Sena, "Exclusive heavy quark photoproduction in *pp*, *pPb* and *PbPb* collisions at the LHC and FCC energies", *Nucl. Phys. A* **1000** (2020) 121862, arXiv:1911.03453 [hep-ph].

[74] S. R. Klein, J. Nystrand, and R. Vogt, "Heavy quark photoproduction in ultraperipheral heavy ion collisions", *Phys. Rev. C* **66** (2002) 044906, arXiv:hep-ph/0206220.

[75] M. Strikman, R. Vogt, and S. N. White, "Probing small x parton densities in ultraperipheral AA and pA collisions at the LHC", *Phys. Rev. Lett.* **96** (2006) 082001, arXiv:hep-ph/0508296.

[76] **CMS** Collaboration, "Technical proposal for a MIP Timing Detector in the CMS experiment Phase 2 upgrade", Tech. Rep. CERN-LHCC-2017-027. LHCC-P-009, CERN, Geneva, Dec, 2017. https://cds.cern.ch/record/2296612.

[77] **CMS** Collaboration, A. Stahl Leiton, "New opportunities in heavy ion physics at HL-LHC with a MIP Timing Detector at CMS", November 2019. https://indico.cern.ch/event/792436/contributions/3535999.

[78] **CMS** Collaboration, V. Khachatryan *et al.*, "Measurement of the total and differential inclusive $B^+$ hadron cross sections in pp collisions at $\sqrt{s} = 13$ TeV", *Phys. Lett. B* **771** (2017) 435–456, arXiv:1609.00873 [hep-ex].

[79] **ATLAS** Collaboration, G. Aad *et al.*, "Measurement of the differential cross-section of $B^+$ meson production in pp collisions at $\sqrt{s} = 7$ TeV at ATLAS", *JHEP* **10** (2013) 042, arXiv:1307.0126 [hep-ex].

[80] P. Buncic, M. Krzewicki, and P. Vande Vyvre, "Technical Design Report for the Upgrade of the Online-Offline Computing System", CDS:CERN-LHCC-2015-006, ALICE-TDR-019. http://cds.cern.ch/record/2011297.

[81] **ALICE** Collaboration, "Evolution of the O2 System",. https://edms.cern.ch/document/2248772/1.

[82] G. Battistoni *et al.*, "Overview of the FLUKA code", *Annals Nucl. Energy* **82** (2015) 10–18.

[83] **ALICE** Collaboration, "Radiation Dose and Fluence in ALICE after LS2, ALICE-PUBLIC-2018-012",. https://cds.cern.ch/record/2642401.

[84] **ALICE** Collaboration, "ALICE ITS Upgrade - Pixel Chip Production Readiness Review", November 2016. https://indico.cern.ch/event/576906.

## A The ALICE Collaboration

S. Acharya[141], D. Adamová[95], A. Adler[74], J. Adolfsson[81], M.M. Aggarwal[100], S. Agha[14], G. Aglieri Rinella[34], M. Agnello[30], N. Agrawal[54,10], Z. Ahammed[141], S. Ahmad[16], S.U. Ahn[76], Z. Akbar[51], A. Akindinov[92], M. Al-Turany[107], S.N. Alam[40], D.S.D. Albuquerque[122], D. Aleksandrov[88], B. Alessandro[59], H.M. Alfanda[6], R. Alfaro Molina[71], B. Ali[16], Y. Ali[14], A. Alici[26,10,54], N. Alizadehvandchali[125], A. Alkin[34,2], J. Alme[21], T. Alt[68], L. Altenkamper[21], I. Altsybeev[113], M.N. Anaam[6], C. Andrei[48], D. Andreou[34], A. Andronic[144], M. Angeletti[34], V. Anguelov[104], T. Antičić[108], F. Antinori[57], P. Antonioli[54], N. Apadula[80], L. Aphecetche[115], H. Appelshäuser[68], S. Arcelli[26], R. Arnaldi[59], M. Arratia[80], I.C. Arsene[20], M. Arslandok[104], A. Augustinus[34], R. Averbeck[107], S. Aziz[78], M.D. Azmi[16], A. Badalà[56], Y.W. Baek[41], S. Bagnasco[59], X. Bai[107], R. Bailhache[68], R. Bala[101], A. Balbino[30], A. Baldisseri[137], M. Ball[43], D. Banerjee[3], R. Barbera[27], L. Barioglio[25], G.G. Barnaföldi[145], L.S. Barnby[94], V. Barret[134], P. Bartalini[6], C. Bartels[127], K. Barth[34], E. Bartsch[68], F. Baruffaldi[28], N. Bastid[134], S. Basu[143], G. Batigne[115], B. Batyunya[75], D. Bauri[49], J.L. Bazo Alba[112], I.G. Bearden[89], C. Beattie[146], I. Belikov[136], A.D.C. Bell Hechavarria[144], F. Bellini[34], R. Bellwied[125], V. Belyaev[93], G. Bencedi[145], S. Beole[25], A. Bercuci[48], Y. Berdnikov[98], A. Berdnikova[104], D. Berenyi[145], R.A. Bertens[130], D. Berzano[59], M.G. Besoiu[67], L. Betev[34], A. Bhasin[101], I.R. Bhat[101], M.A. Bhat[3], H. Bhatt[49], B. Bhattacharjee[42], A. Bianchi[25], L. Bianchi[25], N. Bianchi[52], J. Bielčík[37], J. Bielčíková[95], A. Bilandzic[105], G. Biro[145], S. Biswas[3], J.T. Blair[119], D. Blau[88], C. Blume[68], G. Boca[139], F. Bock[96], A. Bogdanov[93], S. Boi[23], J. Bok[61], L. Boldizsár[145], A. Bolozdynya[93], M. Bombara[38], G. Bonomi[140], H. Borel[137], A. Borissov[93], H. Bossi[146], E. Botta[25], L. Bratrud[68], P. Braun-Munzinger[107], M. Bregant[121], M. Broz[37], E. Bruna[59], G.E. Bruno[106,33], M.D. Buckland[127], D. Budnikov[109], H. Buesching[68], S. Bufalino[30], O. Bugnon[115], P. Buhler[114], P. Buncic[34], Z. Buthelezi[72,131], J.B. Butt[14], S.A. Bysiak[118], D. Caffarri[90], A. Caliva[107], E. Calvo Villar[112], J.M.M. Camacho[120], R.S. Camacho[45], P. Camerini[24], A.A. Capon[114], F. Carnesecchi[26], R. Caron[137], J. Castillo Castellanos[137], A.J. Castro[130], E.A.R. Casula[55], F. Catalano[30], C. Ceballos Sanchez[75], P. Chakraborty[49], S. Chandra[141], W. Chang[6], S. Chapeland[34], M. Chartier[127], S. Chattopadhyay[141], S. Chattopadhyay[110], A. Chauvin[23], C. Cheshkov[135], B. Cheynis[135], V. Chibante Barroso[34], D.D. Chinellato[122], S. Cho[61], P. Chochula[34], P. Christakoglou[90], C.H. Christensen[89], P. Christiansen[81], T. Chujo[133], C. Cicalo[55], L. Cifarelli[10,26], F. Cindolo[54], M.R. Ciupek[107], G. Clai[II,54], J. Cleymans[124], F. Colamaria[53], J.S. Colburn[111], D. Colella[53], A. Collu[80], M. Colocci[26], M. Concas[III,59], G. Conesa Balbastre[79], Z. Conesa del Valle[78], G. Contin[24,60], J.G. Contreras[37], T.M. Cormier[96], Y. Corrales Morales[25], P. Cortese[31], M.R. Cosentino[123], F. Costa[34], S. Costanza[139], P. Crochet[134], E. Cuautle[69], P. Cui[6], L. Cunqueiro[96], T. Dahms[105], A. Dainese[57], F.P.A. Damas[115,137], M.C. Danisch[104], A. Danu[67], D. Das[110], I. Das[110], P. Das[86], P. Das[3], S. Das[3], A. Dash[86], S. Dash[49], S. De[86], A. De Caro[29], G. de Cataldo[53], L. De Cilladi[25], J. de Cuveland[39], A. De Falco[23], D. De Gruttola[10], N. De Marco[59], C. De Martin[24], S. De Pasquale[29], S. Deb[50], H.F. Degenhardt[121], K.R. Deja[142], A. Deloff[85], S. Delsanto[131,25], W. Deng[6], P. Dhankher[49], D. Di Bari[33], A. Di Mauro[34], R.A. Diaz[8], T. Dietel[124], P. Dillenseger[68], Y. Ding[6], R. Divià[34], D.U. Dixit[19], Ø. Djuvsland[21], U. Dmitrieva[62], A. Dobrin[67], B. Dönigus[68], O. Dordic[20], A.K. Dubey[141], A. Dubla[107,90], S. Dudi[100], M. Dukhishyam[86], P. Dupieux[134], R.J. Ehlers[96], V.N. Eikeland[21], D. Elia[53], B. Erazmus[115], F. Erhardt[99], A. Erokhin[113], M.R. Ersdal[21], B. Espagnon[78], G. Eulisse[34], D. Evans[111], S. Evdokimov[91], L. Fabbietti[105], M. Faggin[28], J. Faivre[79], F. Fan[6], A. Fantoni[52], M. Fasel[96], P. Fecchio[30], A. Feliciello[59], G. Feofilov[113], A. Fernández Téllez[45], A. Ferrero[137], A. Ferretti[25], A. Festanti[34], V.J.G. Feuillard[104], J. Figiel[118], S. Filchagin[109], D. Finogeev[62], F.M. Fionda[21], G. Fiorenza[53], F. Flor[125], A.N. Flores[119], S. Foertsch[72], P. Foka[107], S. Fokin[88], E. Fragiacomo[60], U. Frankenfeld[107], U. Fuchs[34], C. Furget[79], A. Furs[62], M. Fusco Girard[29], J.J. Gaardhøje[89], M. Gagliardi[25], A.M. Gago[112], A. Gal[136], C.D. Galvan[120], P. Ganoti[84], C. Garabatos[107], J.R.A. Garcia[45], E. Garcia-Solis[11], K. Garg[115], C. Gargiulo[34], A. Garibli[87], K. Garner[144], P. Gasik[107,105], E.F. Gauger[119], M.B. Gay Ducati[70], M. Germain[115], J. Ghosh[110], P. Ghosh[141], S.K. Ghosh[3], M. Giacalone[26], P. Gianotti[52],

P. Giubellino[107,59], P. Giubilato[28], A.M.C. Glaenzer[137], P. Glässel[104], V. Gonzalez[143,107], L.H. González-Trueba[71], S. Gorbunov[39], L. Görlich[118], A. Goswami[49], S. Gotovac[35], V. Grabski[71], L.K. Graczykowski[142], K.L. Graham[111], L. Greiner[80], A. Grelli[63], C. Grigoras[34], V. Grigoriev[93], A. Grigoryan[I,1], S. Grigoryan[75], O.S. Groettvik[21], F. Grosa[59,30], J.F. Grosse-Oetringhaus[34], R. Grosso[107], R. Guernane[79], M. Guittiere[115], K. Gulbrandsen[89], T. Gunji[132], A. Gupta[101], R. Gupta[101], I.B. Guzman[45], R. Haake[146], M.K. Habib[107], C. Hadjidakis[78], H. Hamagaki[82], G. Hamar[145], M. Hamid[6], R. Hannigan[119], M.R. Haque[86], A. Harlenderova[107], J.W. Harris[146], A. Harton[11], J.A. Hasenbichler[34], H. Hassan[96], Q.U. Hassan[14], D. Hatzifotiadou[54,10], P. Hauer[43], L.B. Havener[146], S. Hayashi[132], S.T. Heckel[105], E. Hellbär[68], H. Helstrup[36], A. Herghelegiu[48], T. Herman[37], E.G. Hernandez[45], G. Herrera Corral[9], F. Herrmann[144], K.F. Hetland[36], H. Hillemanns[34], C. Hills[127], B. Hippolyte[136], B. Hohlweger[105], J. Honermann[144], D. Horak[37], A. Hornung[68], S. Hornung[107], R. Hosokawa[15], P. Hristov[34], C. Huang[78], C. Hughes[130], P. Huhn[68], T.J. Humanic[97], H. Hushnud[110], L.A. Husova[144], N. Hussain[42], S.A. Hussain[14], D. Hutter[39], J.P. Iddon[34,127], R. Ilkaev[109], H. Ilyas[14], M. Inaba[133], G.M. Innocenti[34], M. Ippolitov[88], A. Isakov[95], M.S. Islam[110], M. Ivanov[107], V. Ivanov[98], V. Izucheev[91], B. Jacak[80], N. Jacazio[34,54], P.M. Jacobs[80], S. Jadlovska[117], J. Jadlovsky[117], S. Jaelani[63], C. Jahnke[121], M.J. Jakubowska[142], M.A. Janik[142], T. Janson[74], M. Jercic[99], O. Jevons[111], M. Jin[125], F. Jonas[96,144], P.G. Jones[111], J. Jung[68], M. Jung[68], A. Jusko[111], P. Kalinak[64], A. Kalweit[34], V. Kaplin[93], S. Kar[6], A. Karasu Uysal[77], D. Karatovic[99], O. Karavichev[62], T. Karavicheva[62], P. Karczmarczyk[142], E. Karpechev[62], A. Kazantsev[88], U. Kebschull[74], R. Keidel[47], M. Keil[34], B. Ketzer[43], Z. Khabanova[90], A.M. Khan[6], S. Khan[16], A. Khanzadeev[98], Y. Kharlov[91], A. Khatun[16], A. Khuntia[118], B. Kileng[36], B. Kim[61], B. Kim[133], D. Kim[147], D.J. Kim[126], E.J. Kim[73], H. Kim[17], J. Kim[147], J.S. Kim[41], J. Kim[104], J. Kim[147], J. Kim[73], M. Kim[104], S. Kim[18], T. Kim[147], T. Kim[147], S. Kirsch[68], I. Kisel[39], S. Kiselev[92], A. Kisiel[142], J.L. Klay[5], C. Klein[68], J. Klein[34,59], S. Klein[80], C. Klein-Bösing[144], M. Kleiner[68], T. Klemenz[105], A. Kluge[34], M.L. Knichel[104], A.G. Knospe[125], C. Kobdaj[116], M.K. Köhler[104], T. Kollegger[107], A. Kondratyev[75], N. Kondratyeva[93], E. Kondratyuk[91], J. Konig[68], S.A. Konigstorfer[105], P.J. Konopka[34], G. Kornakov[142], L. Koska[117], O. Kovalenko[85], V. Kovalenko[113], M. Kowalski[118], I. Králik[64], A. Kravčáková[38], L. Kreis[107], M. Krivda[111,64], F. Krizek[95], K. Krizkova Gajdosova[37], M. Krüger[68], E. Kryshen[98], M. Krzewicki[39], V. Kučera[34,61], C. Kuhn[136], P.G. Kuijer[90], L. Kumar[100], S. Kundu[86], P. Kurashvili[85], A. Kurepin[62], A.B. Kurepin[62], A. Kuryakin[109], S. Kushpil[95], J. Kvapil[111], M.J. Kweon[61], J.Y. Kwon[61], Y. Kwon[147], S.L. La Pointe[39], P. La Rocca[27], Y.S. Lai[80], A. Lakrathok[116], M. Lamanna[34], R. Langoy[129], K. Lapidus[34], A. Lardeux[20], P. Larionov[52], E. Laudi[34], R. Lavicka[37], T. Lazareva[113], R. Lea[24], L. Leardini[104], J. Lee[133], S. Lee[147], J. Lehrbach[39], R.C. Lemmon[94], I. León Monzón[120], E.D. Lesser[19], M. Lettrich[34], P. Lévai[145], X. Li[12], X.L. Li[6], J. Lien[129], R. Lietava[111], B. Lim[17], V. Lindenstruth[39], A. Lindner[48], C. Lippmann[107], M.A. Lisa[97], A. Liu[19], J. Liu[127], W.J. Llope[143], I.M. Lofnes[21], V. Loginov[93], C. Loizides[96], P. Loncar[35], J.A. Lopez[104], X. Lopez[134], E. López Torres[8], J.R. Luhder[144], M. Lunardon[28], G. Luparello[60], Y.G. Ma[40], A. Maevskaya[62], M. Mager[34], S.M. Mahmood[20], T. Mahmoud[43], A. Maire[136], R.D. Majka[I,146], M. Malaev[98], Q.W. Malik[20], L. Malinina[IV,75], D. Mal'Kevich[92], P. Malzacher[107], G. Mandaglio[32,56], V. Manko[88], F. Manso[134], V. Manzari[53], Y. Mao[6], M. Marchisone[135], J. Mareš[66], G.V. Margagliotti[24], A. Margotti[54], A. Marín[107], C. Markert[119], M. Marquard[68], N.A. Martin[104], P. Martinengo[34], J.L. Martinez[125], M.I. Martínez[45], G. Martínez García[115], S. Masciocchi[107], M. Masera[25], A. Masoni[55], L. Massacrier[78], A. Mastroserio[138,53], A.M. Mathis[105], O. Matonoha[81], P.F.T. Matuoka[121], A. Matyja[118], C. Mayer[118], F. Mazzaschi[25], M. Mazzilli[53], M.A. Mazzoni[58], A.F. Mechler[68], F. Meddi[22], Y. Melikyan[62], A. Menchaca-Rocha[71], C. Mengke[6], E. Meninno[114,29], A.S. Menon[125], M. Meres[13], S. Mhlanga[124], Y. Miake[133], L. Micheletti[25], L.C. Migliorin[135], D.L. Mihaylov[105], K. Mikhaylov[75,92], A.N. Mishra[69], D. Miśkowiec[107], A. Modak[3], N. Mohammadi[34], A.P. Mohanty[63], B. Mohanty[86], M. Mohisin Khan[V,16], Z. Moravcova[89], C. Mordasini[105], D.A. Moreira De Godoy[144], L.A.P. Moreno[45], I. Morozov[62], A. Morsch[34], T. Mrnjavac[34], V. Muccifora[52], E. Mudnic[35], D. Mühlheim[144], S. Muhuri[141], J.D. Mulligan[80], A. Mulliri[23,55], M.G. Munhoz[121], R.H. Munzer[68], H. Murakami[132], S. Murray[124], L. Musa[34], J. Musinsky[64], C.J. Myers[125], J.W. Myrcha[142], B. Naik[49], R. Nair[85], B.K. Nandi[49],

R. Nania[54,10], E. Nappi[53], M.U. Naru[14], A.F. Nassirpour[81], C. Nattrass[130], R. Nayak[49], T.K. Nayak[86], S. Nazarenko[109], A. Neagu[20], R.A. Negrao De Oliveira[68], L. Nellen[69], S.V. Nesbo[36], G. Neskovic[39], D. Nesterov[113], B.S. Nielsen[89], S. Nikolaev[88], S. Nikulin[88], V. Nikulin[98], F. Noferini[54,10], P. Nomokonov[75], J. Norman[127,79], N. Novitzky[133], P. Nowakowski[142], A. Nyanin[88], J. Nystrand[21], M. Ogino[82], A. Ohlson[81], J. Oleniacz[142], A.C. Oliveira Da Silva[130], M.H. Oliver[146], C. Oppedisano[59], A. Ortiz Velasquez[69], T. Osako[46], A. Oskarsson[81], J. Otwinowski[118], K. Oyama[82], Y. Pachmayer[104], V. Pacik[89], S. Padhan[49], D. Pagano[140], G. Paić[69], J. Pan[143], S. Panebianco[137], P. Pareek[141,50], J. Park[61], J.E. Parkkila[126], S. Parmar[100], S.P. Pathak[125], B. Paul[23], J. Pazzini[140], H. Pei[6], T. Peitzmann[63], X. Peng[6], L.G. Pereira[70], H. Pereira Da Costa[137], D. Peresunko[88], G.M. Perez[8], S. Perrin[137], Y. Pestov[4], V. Petráček[37], M. Petrovici[48], R.P. Pezzi[70], S. Piano[60], M. Pikna[13], P. Pillot[115], O. Pinazza[54,34], L. Pinsky[125], C. Pinto[27], S. Pisano[10,52], D. Pistone[56], M. Płoskoń[80], M. Planinic[99], F. Pliquett[68], M.G. Poghosyan[96], B. Polichtchouk[91], N. Poljak[99], A. Pop[48], S. Porteboeuf-Houssais[134], V. Pozdniakov[75], S.K. Prasad[3], R. Preghenella[54], F. Prino[59], C.A. Pruneau[143], I. Pshenichnov[62], M. Puccio[34], J. Putschke[143], S. Qiu[90], L. Quaglia[25], R.E. Quishpe[125], S. Ragoni[111], S. Raha[3], S. Rajput[101], J. Rak[126], A. Rakotozafindrabe[137], L. Ramello[31], F. Rami[136], S.A.R. Ramirez[45], R. Raniwala[102], S. Raniwala[102], S.S. Räsänen[44], R. Rath[50], I. Ravasenga[90], K.F. Read[96,130], A.R. Redelbach[39], K. Redlich[VI,85], A. Rehman[21], P. Reichelt[68], F. Reidt[34], R. Renfordt[68], Z. Rescakova[38], K. Reygers[104], A. Riabov[98], V. Riabov[98], T. Richert[81,89], M. Richter[20], P. Riedler[34], W. Riegler[34], F. Riggi[27], C. Ristea[67], S.P. Rode[50], M. Rodríguez Cahuantzi[45], K. Røed[20], R. Rogalev[91], E. Rogochaya[75], D. Rohr[34], D. Röhrich[21], P.F. Rojas[45], P.S. Rokita[142], F. Ronchetti[52], A. Rosano[56], E.D. Rosas[69], K. Roslon[142], A. Rossi[57], A. Rotondi[139], A. Roy[50], P. Roy[110], O.V. Rueda[81], R. Rui[24], B. Rumyantsev[75], A. Rustamov[87], E. Ryabinkin[88], Y. Ryabov[98], A. Rybicki[118], H. Rytkonen[126], O.A.M. Saarimaki[44], R. Sadek[115], S. Sadhu[141], S. Sadovsky[91], K. Šafařík[37], S.K. Saha[141], B. Sahoo[49], P. Sahoo[49], R. Sahoo[50], S. Sahoo[65], P.K. Sahu[65], J. Saini[141], S. Sakai[133], S. Sambyal[101], V. Samsonov[98,93], D. Sarkar[143], N. Sarkar[141], P. Sarma[42], V.M. Sarti[105], M.H.P. Sas[63], E. Scapparone[54], J. Schambach[119], H.S. Scheid[68], C. Schiaua[48], R. Schicker[104], A. Schmah[104], C. Schmidt[107], H.R. Schmidt[103], M.O. Schmidt[104], M. Schmidt[103], N.V. Schmidt[96,68], A.R. Schmier[130], J. Schukraft[89], Y. Schutz[136], K. Schwarz[107], K. Schweda[107], G. Scioli[26], E. Scomparin[59], J.E. Seger[15], Y. Sekiguchi[132], D. Sekihata[132], I. Selyuzhenkov[107,93], S. Senyukov[136], D. Serebryakov[62], L. Šerkšnyte[105], A. Sevcenco[67], A. Shabanov[62], A. Shabetai[115], R. Shahoyan[34], W. Shaikh[110], A. Shangaraev[91], A. Sharma[100], A. Sharma[101], H. Sharma[118], M. Sharma[101], N. Sharma[100], S. Sharma[101], O. Sheibani[125], A.I. Sheikh[141], K. Shigaki[46], M. Shimomura[83], S. Shirinkin[92], Q. Shou[40], Y. Sibiriak[88], S. Siddhanta[55], T. Siemiarczuk[85], D. Silvermyr[81], G. Simatovic[90], G. Simonetti[34], B. Singh[105], R. Singh[86], R. Singh[101], R. Singh[50], V.K. Singh[141], V. Singhal[141], T. Sinha[110], B. Sitar[13], M. Sitta[31], T.B. Skaali[20], M. Slupecki[44], N. Smirnov[146], R.J.M. Snellings[63], T.W. Snellman[126], C. Soncco[112], J. Song[125], A. Songmoolnak[116], F. Soramel[28], S. Sorensen[130], I. Sputowska[118], J. Stachel[104], I. Stan[67], P.J. Steffanic[130], E. Stenlund[81], S.F. Stiefelmaier[104], D. Stocco[115], M.M. Storetvedt[36], L.D. Stritto[29], C.P. Stylianidis[90], A.A.P. Suaide[121], T. Sugitate[46], C. Suire[78], M. Suleymanov[14], M. Suljic[34], R. Sultanov[92], M. Šumbera[95], V. Sumberia[101], S. Sumowidagdo[51], S. Swain[65], A. Szabo[13], I. Szarka[13], U. Tabassam[14], S.F. Taghavi[105], G. Taillepied[134], J. Takahashi[122], G.J. Tambave[21], S. Tang[134,6], M. Tarhini[115], M.G. Tarzila[48], A. Tauro[34], G. Tejeda Muñoz[45], A. Telesca[34], L. Terlizzi[25], C. Terrevoli[125], S. Thakur[141], D. Thomas[119], F. Thoresen[89], R. Tieulent[135], A. Tikhonov[62], A.R. Timmins[125], A. Toia[68], N. Topilskaya[62], M. Toppi[52], F. Torales-Acosta[19], S.R. Torres[37], A. Trifiró[32,56], S. Tripathy[69,50], T. Tripathy[49], S. Trogolo[28], G. Trombetta[33], L. Tropp[38], V. Trubnikov[2], W.H. Trzaska[126], T.P. Trzcinski[142], B.A. Trzeciak[37,63], A. Tumkin[109], R. Turrisi[57], T.S. Tveter[20], K. Ullaland[21], E.N. Umaka[125], A. Uras[135], G.L. Usai[23], M. Vala[38], N. Valle[139], S. Vallero[59], N. van der Kolk[63], L.V.R. van Doremalen[63], M. van Leeuwen[63], P. Vande Vyvre[34], D. Varga[145], Z. Varga[145], M. Varga-Kofarago[145], A. Vargas[45], M. Vasileiou[84], A. Vasiliev[88], O. Vázquez Doce[105], V. Vechernin[113], E. Vercellin[25], S. Vergara Limón[45], L. Vermunt[63], R. Vernet[7], R. Vértesi[145], M. Verweij[63], L. Vickovic[35], Z. Vilakazi[131], O. Villalobos Baillie[111], G. Vino[53], A. Vinogradov[88],

T. Virgili[29], V. Vislavicius[89], A. Vodopyanov[75], B. Volkel[34], M.A. Völkl[103], K. Voloshin[92], S.A. Voloshin[143], G. Volpe[33], B. von Haller[34], I. Vorobyev[105], D. Voscek[117], J. Vrláková[38], B. Wagner[21], M. Weber[114], S.G. Weber[144], A. Wegrzynek[34], S.C. Wenzel[34], J.P. Wessels[144], J. Wiechula[68], J. Wikne[20], G. Wilk[85], J. Wilkinson[10], G.A. Willems[144], E. Willsher[111], B. Windelband[104], M. Winn[137], W.E. Witt[130], J.R. Wright[119], Y. Wu[128], R. Xu[6], S. Yalcin[77], Y. Yamaguchi[46], K. Yamakawa[46], S. Yang[21], S. Yano[46,137], Z. Yin[6], H. Yokoyama[63], I.-K. Yoo[17], J.H. Yoon[61], S. Yuan[21], A. Yuncu[104], V. Yurchenko[2], V. Zaccolo[24], A. Zaman[14], C. Zampolli[34], H.J.C. Zanoli[63], N. Zardoshti[34], A. Zarochentsev[113], P. Závada[66], N. Zaviyalov[109], H. Zbroszczyk[142], M. Zhalov[98], S. Zhang[40], X. Zhang[6], Z. Zhang[6], V. Zherebchevskii[113], Y. Zhi[12], D. Zhou[6], Y. Zhou[89], J. Zhu[6,107], Y. Zhu[6], A. Zichichi[10,26], G. Zinovjev[2], N. Zurlo[140]

## Affiliation Notes

[I] Deceased
[II] Also at: Italian National Agency for New Technologies, Energy and Sustainable Economic Development (ENEA), Bologna, Italy
[III] Also at: Dipartimento DET del Politecnico di Torino, Turin, Italy
[IV] Also at: M.V. Lomonosov Moscow State University, D.V. Skobeltsyn Institute of Nuclear, Physics, Moscow, Russia
[V] Also at: Department of Applied Physics, Aligarh Muslim University, Aligarh, India
[VI] Also at: Institute of Theoretical Physics, University of Wroclaw, Poland

## Collaboration Institutes

[1] A.I. Alikhanyan National Science Laboratory (Yerevan Physics Institute) Foundation, Yerevan, Armenia
[2] Bogolyubov Institute for Theoretical Physics, National Academy of Sciences of Ukraine, Kiev, Ukraine
[3] Bose Institute, Department of Physics and Centre for Astroparticle Physics and Space Science (CAPSS), Kolkata, India
[4] Budker Institute for Nuclear Physics, Novosibirsk, Russia
[5] California Polytechnic State University, San Luis Obispo, California, United States
[6] Central China Normal University, Wuhan, China
[7] Centre de Calcul de l'IN2P3, Villeurbanne, Lyon, France
[8] Centro de Aplicaciones Tecnológicas y Desarrollo Nuclear (CEADEN), Havana, Cuba
[9] Centro de Investigación y de Estudios Avanzados (CINVESTAV), Mexico City and Mérida, Mexico
[10] Centro Fermi - Museo Storico della Fisica e Centro Studi e Ricerche "Enrico Fermi', Rome, Italy
[11] Chicago State University, Chicago, Illinois, United States
[12] China Institute of Atomic Energy, Beijing, China
[13] Comenius University Bratislava, Faculty of Mathematics, Physics and Informatics, Bratislava, Slovakia
[14] COMSATS University Islamabad, Islamabad, Pakistan
[15] Creighton University, Omaha, Nebraska, United States
[16] Department of Physics, Aligarh Muslim University, Aligarh, India
[17] Department of Physics, Pusan National University, Pusan, Republic of Korea
[18] Department of Physics, Sejong University, Seoul, Republic of Korea
[19] Department of Physics, University of California, Berkeley, California, United States
[20] Department of Physics, University of Oslo, Oslo, Norway

[21] Department of Physics and Technology, University of Bergen, Bergen, Norway
[22] Dipartimento di Fisica dell'Università 'La Sapienza' and Sezione INFN, Rome, Italy
[23] Dipartimento di Fisica dell'Università and Sezione INFN, Cagliari, Italy
[24] Dipartimento di Fisica dell'Università and Sezione INFN, Trieste, Italy
[25] Dipartimento di Fisica dell'Università and Sezione INFN, Turin, Italy
[26] Dipartimento di Fisica e Astronomia dell'Università and Sezione INFN, Bologna, Italy
[27] Dipartimento di Fisica e Astronomia dell'Università and Sezione INFN, Catania, Italy
[28] Dipartimento di Fisica e Astronomia dell'Università and Sezione INFN, Padova, Italy
[29] Dipartimento di Fisica 'E.R. Caianiello' dell'Università and Gruppo Collegato INFN, Salerno, Italy
[30] Dipartimento DISAT del Politecnico and Sezione INFN, Turin, Italy
[31] Dipartimento di Scienze e Innovazione Tecnologica dell'Università del Piemonte Orientale and INFN Sezione di Torino, Alessandria, Italy
[32] Dipartimento di Scienze MIFT, Università di Messina, Messina, Italy
[33] Dipartimento Interateneo di Fisica 'M. Merlin' and Sezione INFN, Bari, Italy
[34] European Organization for Nuclear Research (CERN), Geneva, Switzerland
[35] Faculty of Electrical Engineering, Mechanical Engineering and Naval Architecture, University of Split, Split, Croatia
[36] Faculty of Engineering and Science, Western Norway University of Applied Sciences, Bergen, Norway
[37] Faculty of Nuclear Sciences and Physical Engineering, Czech Technical University in Prague, Prague, Czech Republic
[38] Faculty of Science, P.J. Šafárik University, Košice, Slovakia
[39] Frankfurt Institute for Advanced Studies, Johann Wolfgang Goethe-Universität Frankfurt, Frankfurt, Germany
[40] Fudan University, Shanghai, China
[41] Gangneung-Wonju National University, Gangneung, Republic of Korea
[42] Gauhati University, Department of Physics, Guwahati, India
[43] Helmholtz-Institut für Strahlen- und Kernphysik, Rheinische Friedrich-Wilhelms-Universität Bonn, Bonn, Germany
[44] Helsinki Institute of Physics (HIP), Helsinki, Finland
[45] High Energy Physics Group, Universidad Autónoma de Puebla, Puebla, Mexico
[46] Hiroshima University, Hiroshima, Japan
[47] Hochschule Worms, Zentrum für Technologietransfer und Telekommunikation (ZTT), Worms, Germany
[48] Horia Hulubei National Institute of Physics and Nuclear Engineering, Bucharest, Romania
[49] Indian Institute of Technology Bombay (IIT), Mumbai, India
[50] Indian Institute of Technology Indore, Indore, India
[51] Indonesian Institute of Sciences, Jakarta, Indonesia
[52] INFN, Laboratori Nazionali di Frascati, Frascati, Italy
[53] INFN, Sezione di Bari, Bari, Italy
[54] INFN, Sezione di Bologna, Bologna, Italy
[55] INFN, Sezione di Cagliari, Cagliari, Italy
[56] INFN, Sezione di Catania, Catania, Italy
[57] INFN, Sezione di Padova, Padova, Italy
[58] INFN, Sezione di Roma, Rome, Italy
[59] INFN, Sezione di Torino, Turin, Italy
[60] INFN, Sezione di Trieste, Trieste, Italy
[61] Inha University, Incheon, Republic of Korea
[62] Institute for Nuclear Research, Academy of Sciences, Moscow, Russia
[63] Institute for Subatomic Physics, Utrecht University/Nikhef, Utrecht, Netherlands

[64] Institute of Experimental Physics, Slovak Academy of Sciences, Košice, Slovakia
[65] Institute of Physics, Homi Bhabha National Institute, Bhubaneswar, India
[66] Institute of Physics of the Czech Academy of Sciences, Prague, Czech Republic
[67] Institute of Space Science (ISS), Bucharest, Romania
[68] Institut für Kernphysik, Johann Wolfgang Goethe-Universität Frankfurt, Frankfurt, Germany
[69] Instituto de Ciencias Nucleares, Universidad Nacional Autónoma de México, Mexico City, Mexico
[70] Instituto de Física, Universidade Federal do Rio Grande do Sul (UFRGS), Porto Alegre, Brazil
[71] Instituto de Física, Universidad Nacional Autónoma de México, Mexico City, Mexico
[72] iThemba LABS, National Research Foundation, Somerset West, South Africa
[73] Jeonbuk National University, Jeonju, Republic of Korea
[74] Johann-Wolfgang-Goethe Universität Frankfurt Institut für Informatik, Fachbereich Informatik und Mathematik, Frankfurt, Germany
[75] Joint Institute for Nuclear Research (JINR), Dubna, Russia
[76] Korea Institute of Science and Technology Information, Daejeon, Republic of Korea
[77] KTO Karatay University, Konya, Turkey
[78] Laboratoire de Physique des 2 Infinis, Irène Joliot-Curie, Orsay, France
[79] Laboratoire de Physique Subatomique et de Cosmologie, Université Grenoble-Alpes, CNRS-IN2P3, Grenoble, France
[80] Lawrence Berkeley National Laboratory, Berkeley, California, United States
[81] Lund University Department of Physics, Division of Particle Physics, Lund, Sweden
[82] Nagasaki Institute of Applied Science, Nagasaki, Japan
[83] Nara Women's University (NWU), Nara, Japan
[84] National and Kapodistrian University of Athens, School of Science, Department of Physics , Athens, Greece
[85] National Centre for Nuclear Research, Warsaw, Poland
[86] National Institute of Science Education and Research, Homi Bhabha National Institute, Jatni, India
[87] National Nuclear Research Center, Baku, Azerbaijan
[88] National Research Centre Kurchatov Institute, Moscow, Russia
[89] Niels Bohr Institute, University of Copenhagen, Copenhagen, Denmark
[90] Nikhef, National institute for subatomic physics, Amsterdam, Netherlands
[91] NRC Kurchatov Institute IHEP, Protvino, Russia
[92] NRC «Kurchatov»Institute - ITEP, Moscow, Russia
[93] NRNU Moscow Engineering Physics Institute, Moscow, Russia
[94] Nuclear Physics Group, STFC Daresbury Laboratory, Daresbury, United Kingdom
[95] Nuclear Physics Institute of the Czech Academy of Sciences, Řež u Prahy, Czech Republic
[96] Oak Ridge National Laboratory, Oak Ridge, Tennessee, United States
[97] Ohio State University, Columbus, Ohio, United States
[98] Petersburg Nuclear Physics Institute, Gatchina, Russia
[99] Physics department, Faculty of science, University of Zagreb, Zagreb, Croatia
[100] Physics Department, Panjab University, Chandigarh, India
[101] Physics Department, University of Jammu, Jammu, India
[102] Physics Department, University of Rajasthan, Jaipur, India
[103] Physikalisches Institut, Eberhard-Karls-Universität Tübingen, Tübingen, Germany
[104] Physikalisches Institut, Ruprecht-Karls-Universität Heidelberg, Heidelberg, Germany
[105] Physik Department, Technische Universität München, Munich, Germany
[106] Politecnico di Bari and Sezione INFN, Bari, Italy
[107] Research Division and ExtreMe Matter Institute EMMI, GSI Helmholtzzentrum für Schwerionenforschung GmbH, Darmstadt, Germany
[108] Rudjer Bošković Institute, Zagreb, Croatia
[109] Russian Federal Nuclear Center (VNIIEF), Sarov, Russia

[110] Saha Institute of Nuclear Physics, Homi Bhabha National Institute, Kolkata, India
[111] School of Physics and Astronomy, University of Birmingham, Birmingham, United Kingdom
[112] Sección Física, Departamento de Ciencias, Pontificia Universidad Católica del Perú, Lima, Peru
[113] St. Petersburg State University, St. Petersburg, Russia
[114] Stefan Meyer Institut für Subatomare Physik (SMI), Vienna, Austria
[115] SUBATECH, IMT Atlantique, Université de Nantes, CNRS-IN2P3, Nantes, France
[116] Suranaree University of Technology, Nakhon Ratchasima, Thailand
[117] Technical University of Košice, Košice, Slovakia
[118] The Henryk Niewodniczanski Institute of Nuclear Physics, Polish Academy of Sciences, Cracow, Poland
[119] The University of Texas at Austin, Austin, Texas, United States
[120] Universidad Autónoma de Sinaloa, Culiacán, Mexico
[121] Universidade de São Paulo (USP), São Paulo, Brazil
[122] Universidade Estadual de Campinas (UNICAMP), Campinas, Brazil
[123] Universidade Federal do ABC, Santo Andre, Brazil
[124] University of Cape Town, Cape Town, South Africa
[125] University of Houston, Houston, Texas, United States
[126] University of Jyväskylä, Jyväskylä, Finland
[127] University of Liverpool, Liverpool, United Kingdom
[128] University of Science and Technology of China, Hefei, China
[129] University of South-Eastern Norway, Tonsberg, Norway
[130] University of Tennessee, Knoxville, Tennessee, United States
[131] University of the Witwatersrand, Johannesburg, South Africa
[132] University of Tokyo, Tokyo, Japan
[133] University of Tsukuba, Tsukuba, Japan
[134] Université Clermont Auvergne, CNRS/IN2P3, LPC, Clermont-Ferrand, France
[135] Université de Lyon, Université Lyon 1, CNRS/IN2P3, IPN-Lyon, Villeurbanne, Lyon, France
[136] Université de Strasbourg, CNRS, IPHC UMR 7178, F-67000 Strasbourg, France, Strasbourg, France
[137] Université Paris-Saclay Centre d'Etudes de Saclay (CEA), IRFU, Départment de Physique Nucléaire (DPhN), Saclay, France
[138] Università degli Studi di Foggia, Foggia, Italy
[139] Università degli Studi di Pavia and Sezione INFN, Pavia, Italy
[140] Università di Brescia and Sezione INFN, Brescia, Italy
[141] Variable Energy Cyclotron Centre, Homi Bhabha National Institute, Kolkata, India
[142] Warsaw University of Technology, Warsaw, Poland
[143] Wayne State University, Detroit, Michigan, United States
[144] Westfälische Wilhelms-Universität Münster, Institut für Kernphysik, Münster, Germany
[145] Wigner Research Centre for Physics, Budapest, Hungary
[146] Yale University, New Haven, Connecticut, United States
[147] Yonsei University, Seoul, Republic of Korea